Technobius

A peer-reviewed open-access journal

Editor-in-Chief:

Yelbek Utepov, PhD, Professor, Department of Civil Engineering, L.N. Gumilyov Eurasian National University, Astana, Kazakhstan

Technical Editor:

Assel Tulebekova, PhD, Associate Professor, Department of Civil Engineering, L.N. Gumilyov Eurasian National University, Astana, Kazakhstan

Editors:

Yuri Pukharenko, Doctor of Technical Sciences, Professor, Department of Building Materials Technology and Metrology, Saint Petersburg State University of Architecture and Civil Engineering, Saint Petersburg, Russian Federation

Askar Zhussupbekov, Doctor of Technical Sciences, Professor, Department of Civil Engineering, L.N. Gumilyov Eurasian National University, Astana, Kazakhstan

Evgeniya Tkach, Doctor of Technical Sciences, Professor, Department of Building Materials Science, Moscow State University of Civil Engineering, Moscow, Russian Federation

Ignacio Menéndez Pidal de Navascués, Doctor of Technical Sciences, Professor, Department of Civil Engineering, Technical University of Madrid, Madrid, Spain

Irina Aubakirova, Candidate of Technical Sciences, Associate Professor, Department of Building Materials Technology and Metrology, Saint Petersburg State University of Architecture and Civil Engineering, Saint Petersburg, Russian Federation

Zeljko Kos, PhD, Assistant Professor, Department of Civil Engineering, University North, Varaždin, Croatia

Aleksej Aniskin, Candidate of Technical Sciences, Assistant Professor, Department of Civil Engineering, University North, Varaždin, Croatia

Daniyar Akhmetov, Doctor of Technical Sciences, Associate Professor, Department of Construction and Building materials, Satbayev University, Almaty, Kazakhstan

Zhanbolat Shakhmov, PhD, Associate Professor, Department of Civil Engineering, L.N. Gumilyov Eurasian National University, Astana, Kazakhstan

Timoth Mkilima, PhD, Lecturer, Department of Environmental Engineering and Management, the University of Dodoma, Dodoma, Tanzania

Aliya Aldungarova, PhD, Associate Professor, School of Architecture, Civil Engineering and Energy, D. Serikbayev East Kazakhstan technical university, Ust-Kamenogorsk, Kazakhstan

CONTENTS

Technobius

Article

Foundation for waterlogged bases with conical void design

Assel Mukhamejanova[1,*], Kalamkas Abdrakhmanova[2], Shamshygaiyn Toleubayeva[3], Aigul Kozhas[3]

[1]Department of Civil Engineering, L.N. Gumilyov Eurasian National University, Astana, Kazakhstan
[2]Department of Civil Engineering, Abylkas Saginov Karaganda Technical University, Karaganda, Kazakhstan
[3]Department of Technology of Industrial and Civil Engineering, L.N. Gumilyov Eurasian National University, Astana, Kazakhstan
*Correspondence: assel.84@list.ru

Abstract. The article presents hollow foundations that play a multifunctional role: drainage to accelerate the process of consolidation of weak water-saturated cohesive foundation soils, drainage in case of obvious underflooding, anti-barrage in case of latent underflooding, as well as compensating for possible swelling or frost heaving of the clay soils. The adopted design solution makes it possible to transfer the load from the foundation to the soil foundation that includes loose cavity filling material through a more developed support area than a foundation with a flat footing. Unlike the solid foundation, the hollow foundation has a higher bearing capacity by 120 N more, and in the intervals of high loads (> 400 N) the settlement of the hollow foundation develops with an occasional lag from the settlement of the solid foundation. The use of hollow concrete foundations makes it possible to expand the area of application of prefabricated foundations, simplify their manufacture, increase their bearing capacity and ensure their strength and durability, while reducing the material intensity and cost of construction.
Keywords: hollow foundations, resource-saving methods, sediment, roll, existing foundation.

1. Introduction

The use of traditional foundations with a solid waterproof sole causes artificial flooding of the territory (barrage effect), does not ensure operational reliability, since when poorly permeable foundation soils are flooded under unfavorable drainage conditions, there can be a risk of losing the building stability [1].

So far, shallow solid foundations used in construction practice are not economically profitable when building in conditions of heaving soils, swelling clays, especially for relatively light low-rise buildings and engineering structures (power line supports, pipelines, etc.). At this, it is necessary to use traditional labor-intensive, material-intensive sand cushions and other energy-intensive inefficient technologies: replacing the swelling layer, increasing the depth of foundations, arranging pile foundations, etc. The known methods of strengthening foundations and walls with reinforced concrete belts or simple mesh reinforcement in mortar joints are not used due to complexity, labor intensity and high cost for normal construction conditions.

Traditional methods of protecting buried parts of buildings against groundwater using "backfilling of hollows" are not effective in flooding urban areas [2].

In present day conditions of the rapid growth of scientific and technological progress, signs of the ecological crisis of cities have become especially noticeable due to the hidden factors of anthropogenic geological processes, the negative consequences of which have not been considered in advance in traditional methods of surveys, design, technologies of erecting buildings and their operation [3].

For these reasons, in recent years, accidents in residential buildings have occurred in several countries, resulting in the death of people, which indicates the failure of traditional design methods and the need to adopt fundamentally new design, technological solutions to improve the reliability and safety of housing. There is known a foundation including extended downward shaft with a through vertical cavity filled with bulk material [4]. The disadvantage of such a foundation is its acceptability for use only for tower structures erected on rocky soils.

There are known schemes of foundations of rectangular and trapezoidal shape with longitudinal and transverse cavities. The disadvantages of such schemes include the complexity of manufacturing and the unreliability of the foundations, due to the irrational shape and orientation of the cavities in space.

There are known foundation including a rectangular base plate with a through vertical cavity [5]. However, this design is also unreliable in operation, since the area of the sole of the base plate is reduced by the area of the base of the cavity (the sum of the cross-sectional areas of the holes), which leads to decreasing the bearing capacity of the foundation. In addition, the design is difficult to manufacture, uneconomical and requires high material consumption.

There is known a typical prefabricated foundation including a base plate without voids and holes. The disadvantages of this design include its high cost, high resource consumption, bulkiness, and irrational distribution of the specific reactive pressure of the base.

The idea of developing biopositive and environmentally protected buildings adapted to the adverse effects of built-up areas of natural and man-made nature in such a comprehensive target formulation is put forward for the first time and is a major unresolved problem of modern construction, which is of great scientific and practical importance [6].

In the proposed reinforcement method, unlike analogues, there are used elements already present in the design of buildings under construction lintel beams of window and balcony openings, which are a continuous stiffening belt located on each floor along the perimeter of the outer walls of the building.

In the new foundation, unlike analogues, instead of a mesh reinforcement system, there are proposed closed reinforcing loops that work only in tension; moreover, the saved part of the reinforcement is used to reinforce the reinforcement belt, which combines all the elements of the foundation into a single whole and thereby ensures spatial rigidity of the foundation-basement part of the building [7]. Hollow foundations including loose material inside, can be considered as foundations placed on distribution pads, which play a multifunctional role: water discharging to accelerate the process of consolidation (strengthening) of weak water-saturated cohesive base soils; draining with obvious flooding; anti-barrage with hidden flooding; compensating for possible swelling or frost heaving of clay base soils. Moreover, the inner cushions of hollow foundations, unlike traditional soil cushions, have the minimum consumption of the bulk material, since their dimensions are taken constructively. Thus, the method of complex protection of a building developed by the authors, which has an anti-barrage, adaptive effect, is a synthesis of the potential possibilities of the method of strengthening building envelopes, a foundation with a filtering sole and a stiffening belt, as well as the known design solutions for the arrangement of an artificial base layer and near-wall, reservoir drainage [8].

The use of the proposed foundation designs with a filter base guarantees high reliability and environmental protection of the facilities under construction.

The use of hollow foundations instead of traditional solid foundations is also economically beneficial when building in conditions of heaving soils, swelling clays, especially for relatively light low-rise buildings and engineering structures (power line supports, pipelines, etc.). At this, the internal filling of hollow foundations of coarse sand or fine gravel, in addition to the draining function, can also play the role of a compensating (anti-rock) cushion and eliminates the use of traditional labor-intensive, material-intensive sand cushions and other inefficient technologies [9].

The commercial attractiveness of the innovative method of "integrated protection" is to ensure operational reliability of buildings in all possible cases of basement soil flooding: hidden flooding, emergency leaks from utility pipelines, rising groundwater levels [10].

2. Methods

Based on the analysis of the design features of the known prefabricated concrete strip foundations, the authors have developed a concrete hollow foundation design, the essence of which is as follows (see Figure 1). Its dimensions: the height, length, and width of the support block, which has a square shape in plan, are assigned depending on the angle of rigidity, as for rigid foundations. In the central part of the concrete block, where compressive stresses mainly occur, a through cavity is made that expands downwards and is provided with an internal backfill of a loose hard material of dense addition. Moreover, the slope of the side surface of the cavity to the horizontal plane of the base is taken not less than the angle of internal friction of the bulk material. The adopted shape of the hole of the support block contributes to the denser packing of the bulk material grains in the process of filling the foundation cavity and ensures uniform transfer of the load to the soil base including the backfill. The ratio of the area of the lower hole to the total area of the sole of the support block is accepted considering the rational use of the strength characteristics of the foundation materials in the range of 0.5...0.6.

Figure 1a and 1b shows the view of a hollow concrete foundation in plan and section, respectively.
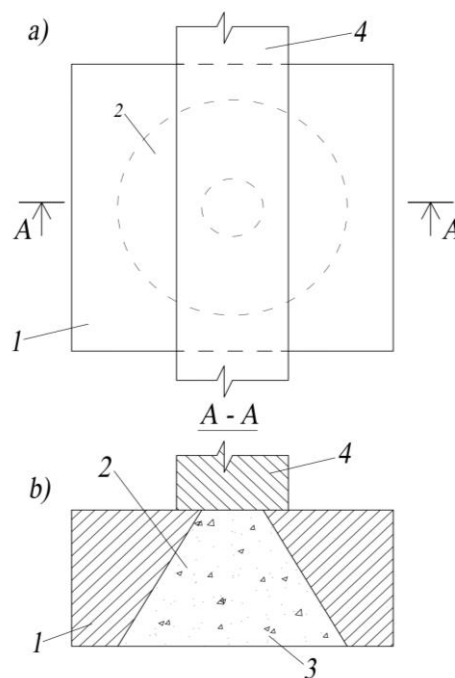
Figure 1 – Hollow concrete foundation: a) Plan; b) Section.

As shown in Figure 1, in the process of manufacturing support block (1), the angle of inclination of the generatrix of cavity (2) to its base is taken as large by 1.1...1.3 of the angle of internal friction of bulk material (3), which can be gravel or wood soil. In this case the area of the base of cavity 2 is assigned within 0.5...0.6 of the total area of support block 1 (which means the entire area of the sole of the support block that does not have a cavity). Support blocks 1 are placed on the sand preparation of the soil base, then cavities 2 are filled with loose material (3), after which foundation blocks (4) are laid.

The adopted design solution allows transferring the load from the foundation to the soil base including the loose material filling the cavity through a more developed bearing area than the foundation with a flat sole. In this case, there is achieved increasing the contact area of two bodies of different rigidity: the hollow concrete block and the soil medium, by more than 20 %. It obviously leads to decreasing the intensity of reactive pressures because of their redistribution within the developed bearing area of the hollow foundation, hence, to the unloading of the concrete

block body. For this purpose, based on the experimental data, it is recommended to keep the ratio of the deformation moduli of the backfill material and the base soil within, which will significantly reduce the concentration of contact reactive pressures arising in the peripheral zone of the hollow foundation block base. One of the main advantages of this design is that the base reaction is manifested not only in the form of vertical frontal resistance, as is typical for traditional foundations with a flat sole but also in the form of friction resistance along the inclined side surface of the inner cavity of the support block. Moreover, the frontal resistance of the soil base during the operation of the foundation occurs in the plane of the sole and top of the support block, as well as along the side surface of the cavity. The geometric parameters (the wall thickness and height) of the hollow support block in two mutually perpendicular directions are taken as variables depending on its stress-strain state for a more complete use of the construction material strength characteristics.

In general, the foundation works as follows. From the beginning of the process of loading the foundation, the work mainly includes the lower horizontal part of the sole of the hollow block (about ~50 % of the bearing area), therefore, the settlement occurs due to compression of the natural foundation soil. As the load on the foundation increases and it subsides, the work will also gradually include the inner side surface of the hollow block (about ~48 % of the bearing area) and the upper horizontal area (~2% of the bearing area). After the foundation is fully loaded and redistributed, stabilization of the reactive pressures of the settlement occurs due to the additional compaction of the backfill material and mainly because of deformation of the natural foundation soil.

The pattern of development of the hollow foundation settlement with increasing the load will differ significantly from that for the traditional solid foundation with a flat sole, which is explained by the absence of a compacted core (wedge) under the center of the loaded area. It is known that the formation of the specified zone of the base is the main reason for the development of uplift of the soil leading to the loss of stability of conventional foundations.

Hollow foundations that include loose material inside, can be considered as foundations placed on distribution pads, which play a multifunctional role: water discharging to accelerate the process of filtration consolidation (compaction) of water-saturated clay soils of the base; draining with obvious flooding; anti-barrage with hidden flooding; compensating for possible swelling or frost heaving of cohesive base soils. Moreover, the internal distribution pads of hollow foundations, unlike traditional soil pads, have the minimum consumption of the bulk material since their dimensions are taken constructively.

The body of a hollow base plate filled with the bulk material, under the action of the reactive pressure of the base soil acts like a rigid retaining wall having a distributed load on the surface of the retained backfill. The correctness of this assumption was confirmed by the results of numerical studies and comparative calculations performed according to the method of designing pile heads.

2.1 Experimental studies of the hollow foundation operation

The purpose of the model experiments is to identify the features of interaction of a hollow foundation with the ground base by carrying out comparative tests. According to the purpose of the studies, when carrying out parallel experiments under identical conditions with models of solid (ordinary) and hollow base plates, the following tasks were set:

1) To fix the settlements of experimental foundations under increasing load.

2) To measure the settlement of the ground surface outside the foot area of the loaded stamps.

3) To reveal the nature of the base deformation dependence on the shape of the model foundation base.

2.2 Analyzing the results of model experiments

In the experiments, two types of foundation models were tested:

a) the first type simulated the work of a traditional solid foundation with a hard sole and played the role of a reference sample.

b) the second type was a model of a light-weight hollow foundation with a complex sole design including a rigid and a ground part.

The general view of the model test bench is shown in Figure 2 below.
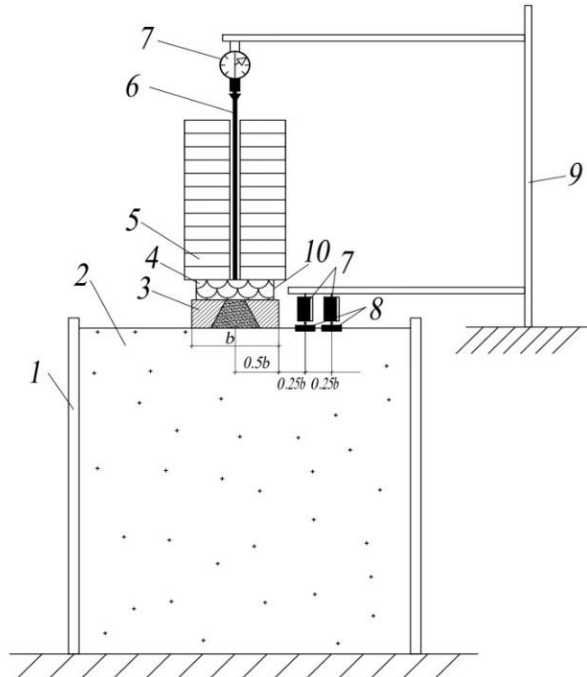
Figure 2 – General view of the model test bench: 1 – Tray; 2 – Soil (fine sand); 3 – Foundation model (stamp); 4 – Wooden gasket; 5 – Weights on the stamp; 6 – Steel string; 7 – Indicators; 8 – Surface marks; 9 – Reference system; 10 – Filling material (coarse sand)

According to the purpose and objectives of the experiment, the loaded stamps were measured, as well as the ground surface near the stamps at the distance of 0.25 b and 0.5 b from their outer edge, where b is the width of the stamp sole. In the experiments, the stamps were loaded in stages until the bearing capacity of the base was completely exhausted.

3. Results and Discussion

The settlement of hollow and solid foundation models' dependences on loads are shown in Figure 3a and 3b. Summary graphs of the development of settlements of experimental foundations with increasing vertical load on the base are shown in Figure 4.

a) graphs of the solid foundation model settlement

b) graphs of the hollow foundation model settlement
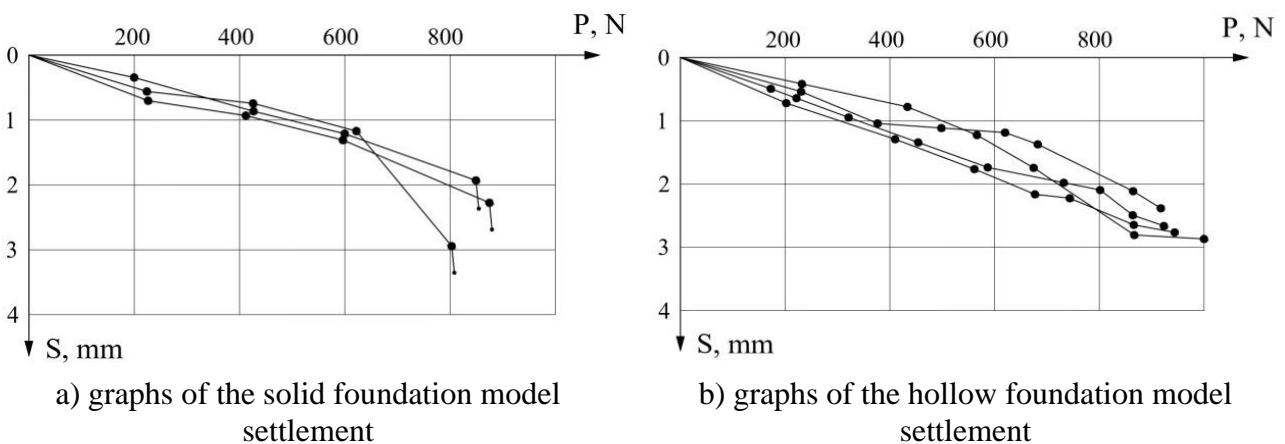
Figure 3 – Dependence of hollow and solid foundation model settlement on loads
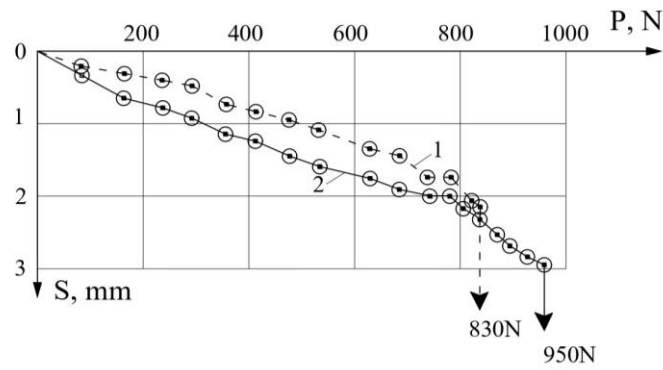
Figure 4 – Dependence of hollow and solid foundation model settlement on loads: 1 – for the solid foundation model; 2 – for the hollow foundation model

The graphs of the settlements of stamps and the soil surface of the base development outside the area of their foot at individual stages of loading are shown in Figures 5 and 6.
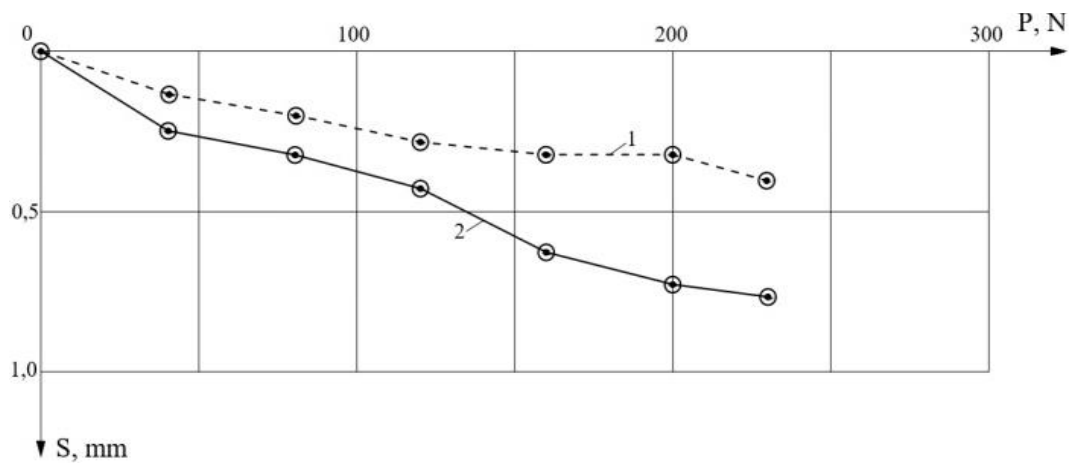
a) At the load range of 0...230 N
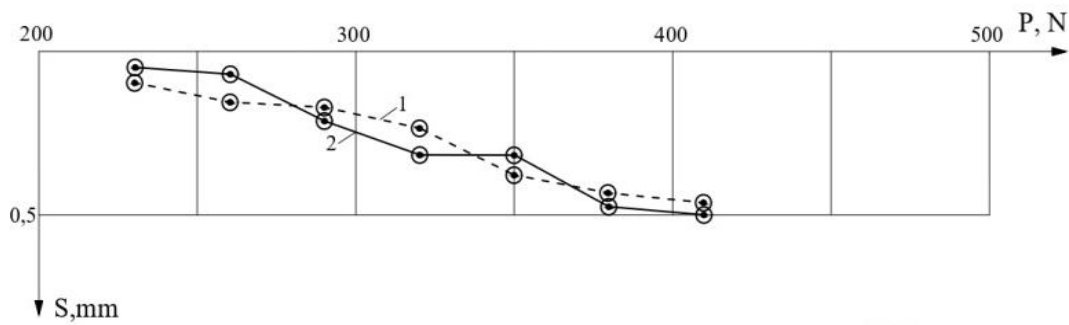
b) At the load range of 230...410 N
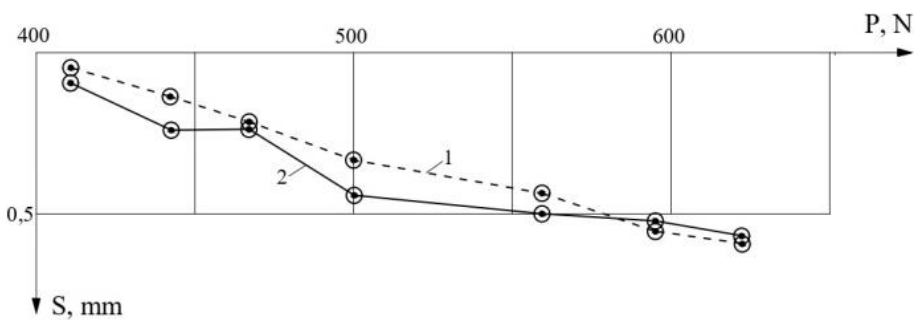
c) At the load range of 410...620 N
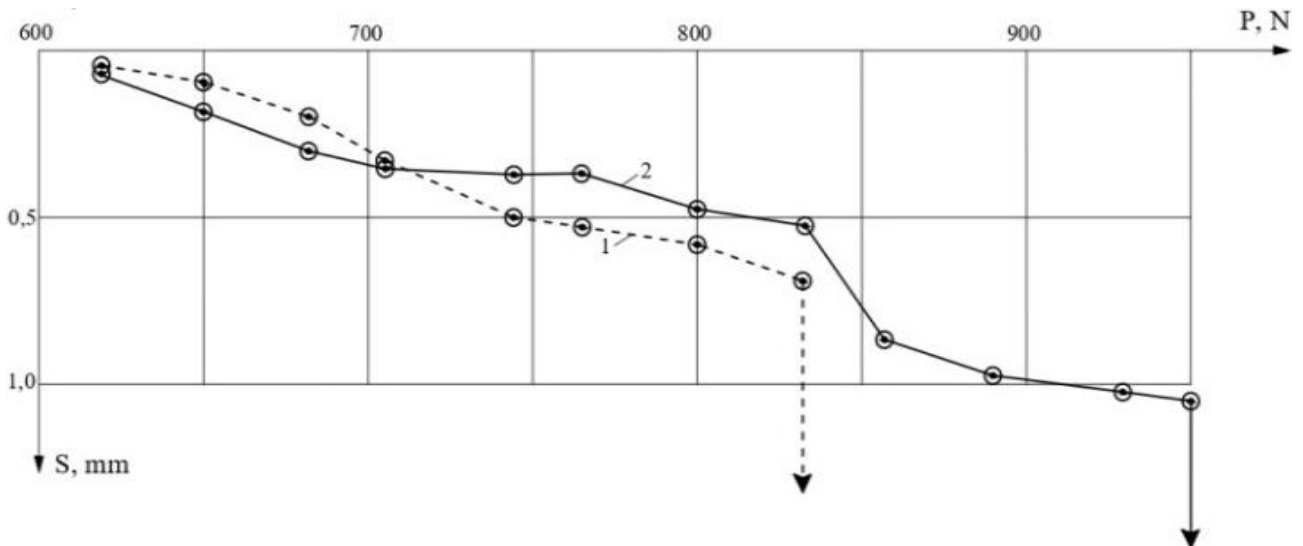
d) At the load range of from 620 N to buckling
Figure 5 – Graphs of the stamp settlements: 1 – For the solid foundation model; 2 – For the hollow foundation model

It is seen from the comparison of curves 1 and 2 (Figure 4 and 5d), the bearing capacity of a hollow foundation is 120 N greater than that of a solid foundation. At the same time, the settlement of a lightweight foundation slightly exceeds that of a solid foundation. To find out the reason for this phenomenon, it is of interest to compare for both models the graphs of the development of stamp settlements and the base surface around them at separate stages of loading.
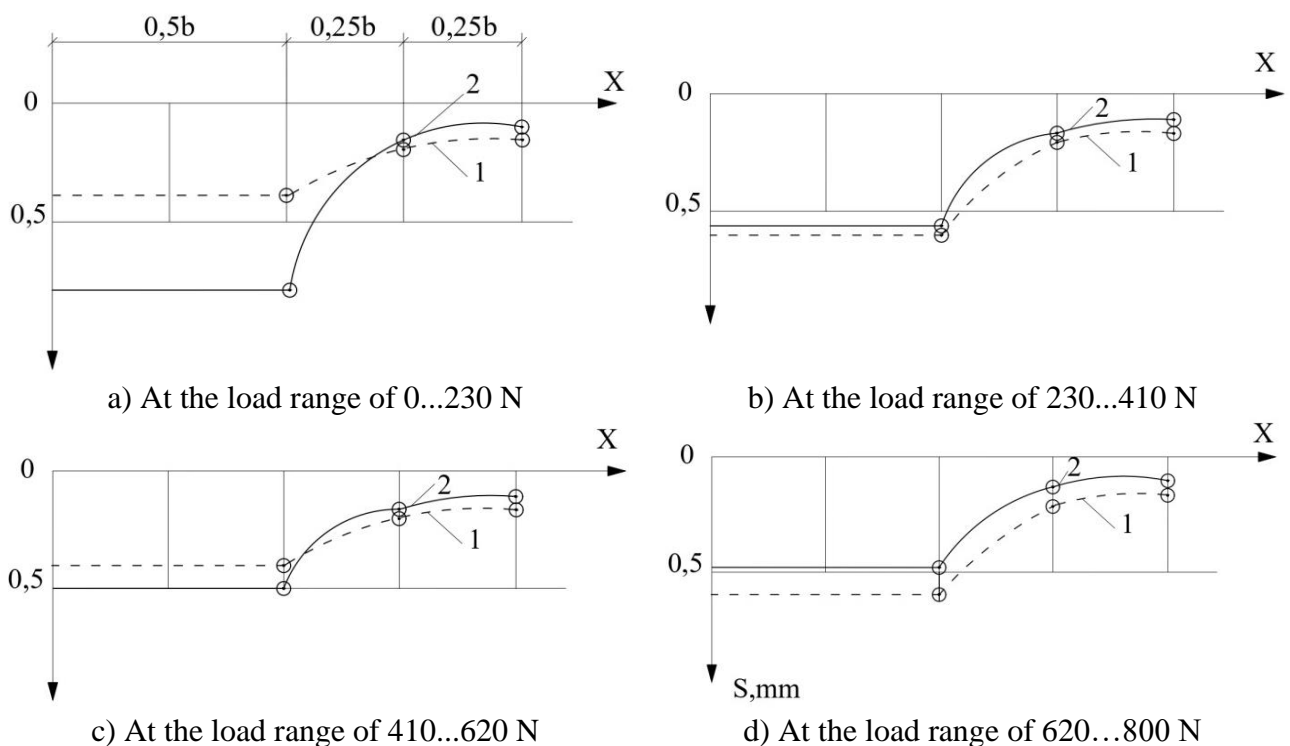
a) At the load range of 0...230 N

b) At the load range of 230...410 N

c) At the load range of 410...620 N

d) At the load range of 620…800 N

Figure 6 – Graphs of the soil surface settlements: 1 – For the solid foundation model; 2 – For hollow foundation model

A comparison of the graphs presented in Figures 5a and 6a show that increasing the settlement of the hollow foundation is caused by the additional compaction of its soil part (filling material) in the initial period of loading in the load range of 0...230 N.

This is clearly seen from the comparison of curves 1 and 2 (Figures 5a and 6a). It is known that the development of a sinkhole around the foundation is one of the main signs of the gradual involvement of the deepest layers of the subgrade into the work. Hence, the position of curve 2 in Figure 6a that is rather different from Figures 6b, 6c and 6d is explained by the cutting into the ground of the rigid peripheral part of the hollow foundation sole as a result of additional compaction of the filling material.

At the next loading stages, the settlement of a hollow foundation develops almost the same as compared to a solid one, which can be seen from the comparison of curves 1 and 2 in Figures 5b, 5c and 5d. It should be noted that at significant loads over 400 N the settlement rate of a hollow foundation is uneven. This is clearly seen from the comparison of curves 1 and 2 in Figures 5c and 5d in the load ranges of 440 N...470 N, 560 N...590 N and 710 N...770 N where the settlement of the hollow foundation (curve 2) practically dies out. This phenomenon is apparently explained by the peculiarities of the nature of interaction with the base of the lightweight foundation, which has a complex shape of the supporting area and the soil part within the base.

4. Conclusions

The analysis of the above phenomena occurring at the base of loaded experimental foundations allows drawing the following conclusions.

1. The total settlement of a hollow foundation, other things being equal, is greater than the settlement of a solid foundation.

2. A slight increase in the settlement of a hollow foundation compared to a solid foundation is due to additional compaction of the material filling the internal cavity in the initial period of loading (in the load range of 0...230 N).

3. Unlike a solid foundation, a hollow foundation has a greater bearing capacity (120 N more).

4. In the intervals of high loads (over 400 N), the settlement of the hollow foundation develops with episodic lagging behind the settlement of the solid foundation.

5. Compared with a solid foundation, the size of the sinkhole around a hollow foundation is smaller.

References

1. Geological Hazards During Construction and Operation of Shallow Subway Stations and Tunnels by the Example of the Kharkiv Metro (1968–2018) / V. Iegupov, G. Strizhelchik, A. Kupreychyk, A. Ubiyvovk // International journal of georesources and environment. — 2018. — Vol. 4, No. 4. — P. 187–200. https://doi.org/10.15273/ijge.2018.04.030
2. Country Area Territory Protection from Flooding; Construction Conditions, Problem Definition and Solution / A. Makarov, A. Mihailova, N. Arefiev, S. Pavlov, T. Chashchina, V. Terleev, V. Badenko // Procedia Engineering. — 2015. — Vol. 117. — P. 225–231. https://doi.org/10.1016/j.proeng.2015.08.153
3. Interaction Analysis of Adjacent Foundations of Renovated Builidngs / E.S. Utenov, A.Zh. Zhusupbekov, S.N. Sotnikov, A.T. Mukhamedzhanova, B.O. Kaldanova // Soil Mechanics and Foundation Engineering. — 2017. — Vol. 54, No. 1. — P. 17–23. https://doi.org/10.1007/s11204-017-9427-7
4. Raschet fundamentov rekonstruiruemyh zdanij / E.S. Utenov // Monograph. — Karaganda: Publishing house of KSTU, 2013. — 237 p.
5. Numerical Analysis of Settling of Foundations of Heightened Buildings by the Modulus-Free Method / E.S. Utenov, A.Zh. Zhusupbekov, K.A. Abdrakhmanova, G.K. Tanyrbergenova, A.T. Mukhamedzhanova // Soil Mechanics and Foundation Engineering. — 2019. — Vol. 56, No. 4. — P. 239–245. https://doi.org/10.1007/s11204-019-09597-4
6. Raschet osnovanij zdanij v usloviyah zastroennyh gorodskih territorij / E.S. Utenov. — Karaganda: Publishing house of KSTU, 2004. — 248 p.
7. Calculation of Building Settlement on Flood-Prone Foundations by Using the Modulus-Free Method / Y.S. Utenov, A.Zh. Zhusupbekov, S.K. Abildin, A.T. Mukhamedzhanova, B.G. Abdrakhmanova // Soil Mechanics and Foundation Engineering. — 2022. — Vol. 59, No. 1. — P. 51–56. https://doi.org/10.1007/s11204-022-09783-x

8. Modern technologies of foundation building in the conditions of weak soils of St. Petersburg / R. Mangushev, S. Sotnikov, A. Osokin // E3S Web of Conferences. — 2020. — Vol. 164. — P. 02018. https://doi.org/10.1051/e3sconf/202016402018
9. Soil Mechanics and Foundation Engineering / Murphy, V.N.S. — New Delhi, India: CBS Publishers and Distributors Pvt., Ltd., 2010.
10. Groundwater Rising as Environmental Problem, Causes and Solutions: Case Study from Aswan City, Upper Egypt / S.A. Selim, A.M. Hamdan, A.A. Rady // Open Journal of Geology. — 2014. — Vol. 04, No. 07. — P. 324–341. https://doi.org/10.4236/ojg.2014.47025

Information about authors:

Assel Mukhamejanova – PhD, Senior Lecturer, Department of Civil Engineering, L.N. Gumilyov Eurasian National University, Astana, Kazakhstan, assel.84@list.ru

Kalamkas Abdrakhmanova – PhD, Senior Lecturer, Department of Civil Engineering, Abylkas Saginov Karaganda Technical University, Karaganda, Kazakhstan, kagaip@mail.ru

Shamshygaiyn Toleubayeva – PhD, Senior Lecturer, Department of Technology of Industrial and Civil Construction, L.N. Gumilyov Eurasian National University, Astana, Kazakhstan, shamshygaiyn@mail.ru

Aigul Kozhas – Candidate of Technical Sciences, Senior Lecturer, Department of Technology of Industrial and Civil Construction, L.N. Gumilyov Eurasian National University, Astana, Kazakhstan, kozhas@bk.ru

Author Contributions:

Assel Mukhamejanova – concept, methodology, drafting, funding acquisition.
Kalamkas Abdrakhmanova – resources, interpretation, analysis.
Shamshygaiyn Toleubayeva – data collection, modeling, testing.
Aigul Kozhas – visualization, editing.

Article

Methodology for determining coordinate points using automated software and aircraft

Zhassulan Kuzbakhov, Shyngys Zharassov*

Department of Civil Engineering, L.N. Gumilyov Eurasian National University, Astana, Kazakhstan
*Correspondence: zhshzh95@gmail.com

Abstract. Engineers are currently facing questions about the use of geographic information systems or software to implement projects in a short time. The problem with using geographic information systems in construction is the relevance of the available data. An example is open sources with satellite images. This problem appeared even before satellite-positioning systems emerged. In this connection, the purpose of this article is to find the deviation of source points when performing photogrammetry with marker detection in Agisoft PhotoScan software. This method of determining coordinates using a single point and its correlation on the ground is applicable in the case of rapid calculations, where the volumes of earth masses are large enough and do not require increased accuracy at the stage of approximate calculations. As a result of the comparison of traditional and automated methods of definition of coordinates on the ground has been found an essential distinction, both in total values and in time spent for the definition of points of coordinates. The considerable difference revealed by the results of the comparison of coordinates is presented in the table as a color gradation. The average deviation between known coordinates and coordinates obtained in Agisoft PhotoScan by axes was: X=0.87%, Y=0.45%, Z=0.12%.
Keywords: Agisoft PhotoScan, surveying, automation, photogrammetry, geodesy, topographic mapping.

1. Introduction

The use of digital tools in automating construction processes is rapidly advancing, despite the challenges posed by the complexity and diversity of these processes. There is a growing interest in leveraging geographic information systems and software to streamline project implementation, which raises questions for engineers about how best to apply these tools within tight timeframes. However, integrating such tools can lead to errors and deviations caused by human mistakes or insufficient information on their practical application [1].

When it comes to using geographic information systems in construction, the main challenge is the quality and relevance of the available data. For instance, open sources like satellite images may be of limited use due to their quality, coverage, and the current state of urbanization in the area being assessed. This can make it difficult to accurately evaluate the situation for construction projects [2].

Although surveying a plane with a GPS receiver is relatively straightforward, those who use optical and satellite instruments should be aware of the potential challenges associated with these tools. Attempting to integrate traditional and satellite surveying instruments can lead to several points for consideration [3], including:
- The coordinate system used when taking pictures;
- Relativity surface;
- Scale factor of the projection;
- Correction for projection height, etc.

This issue has been a challenge even prior to the advent of satellite positioning systems. For example, when using high-precision total stations of the Leica series, it was found that the deviation was about 0.2 meters, factoring in the coordinate system adopted in the region being surveyed. This deviation occurs despite considering the installation of the device and the position of the reflector. It's important to note that Leica GPS receivers typically determine the coordinates of points in the WGS-84 geodetic coordinate system. However, in practice, the UTM32 coordinate system is used when converting to plane coordinates, which establishes the relationship between the ellipsoid surface part and the plane coordinates in the projection. Different results can be obtained by using a Leica TPS total station (Figure 1), which determines the coordinates over a peg. Measurements taken with a reflector can also have significant errors if the ellipsoid surface is not taken into account [4].
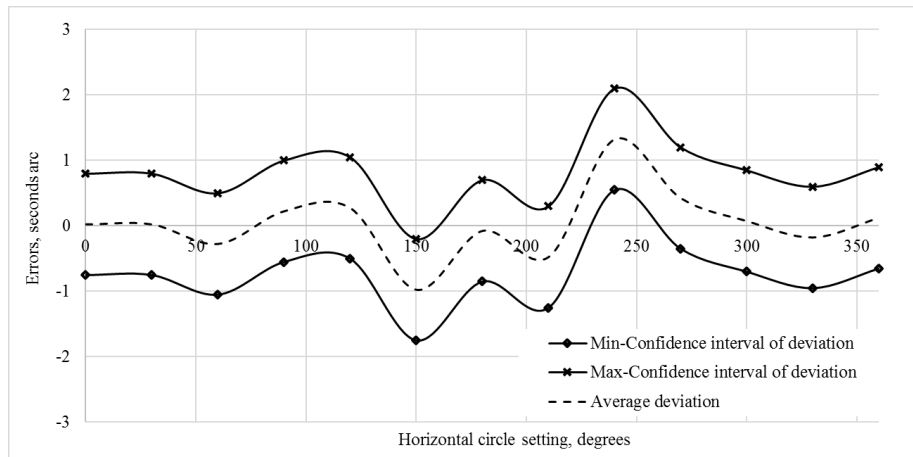
Figure 1 – Tachymeter accuracy Leica TSO06 [4]

Moreover, there are software programs available that can automate surface breakdowns by correlating points based on surface topography. However, deviations in these measurements can lead to unpredictable consequences, as minimum and maximum values can significantly affect the accuracy of the results [5]. The accuracy of the measuring instrument used, as well as other factors such as image quality, weather conditions, and the skill of the operator flying drones or other aircraft, are critical considerations in automating the surveying process [6].

Therefore, the objective of this article is to determine the deviation of baseline points when conducting photogrammetry using marker detection in the Agisoft PhotoScan software. Agisoft PhotoScan is primarily an autonomous software tool that can conduct photogrammetric processing of digital images and generate three-dimensional spatial data for use in Geographic Information Systems (GIS). Therefore, the authors of this article showcase an example of executing topographic surveys using this software. The example pertains to a ground excavation site, which was utilized for embankment or excavation during the construction of residential complexes [7].

2. Methods

The method used in this study to determine coordinates involves using a single point and its correlation on the ground, which is suitable for quick calculations when the volume of earth masses is sufficiently large and high accuracy is not required at the stage of approximate calculations.

For this study, Agisoft PhotoScan software was utilized. In addition to the advantages previously mentioned, an additional benefit of using stand-alone software is its flexibility and adaptability to various systems for calculations.

The drone used in this study for photogrammetry is the Quadcopter DJI Mini 3 Pro. The selection of this model was based on the manufacturer's specifications, with special emphasis on the matrix size and resolution of the captured frames. Additionally, the number of frames captured and the time of day of shooting are critical factors to consider. A higher number of frames captured

enables the accurate construction of a 3D model, while the absence of shadow zones facilitates the calculation of surface relief [8].

The survey process is illustrated in Figure 2 below. The drone's trajectory for mapping the terrain can follow a continuous circular motion around the center or the edge of the surveyed area, or move along a path from the beginning to the end of the polygon within the defined boundaries of the area. The captured images are aligned with a certain degree of accuracy, where the orientation of each image is tied to the angle of view of the drone's camera, resulting in the creation of a point cloud.
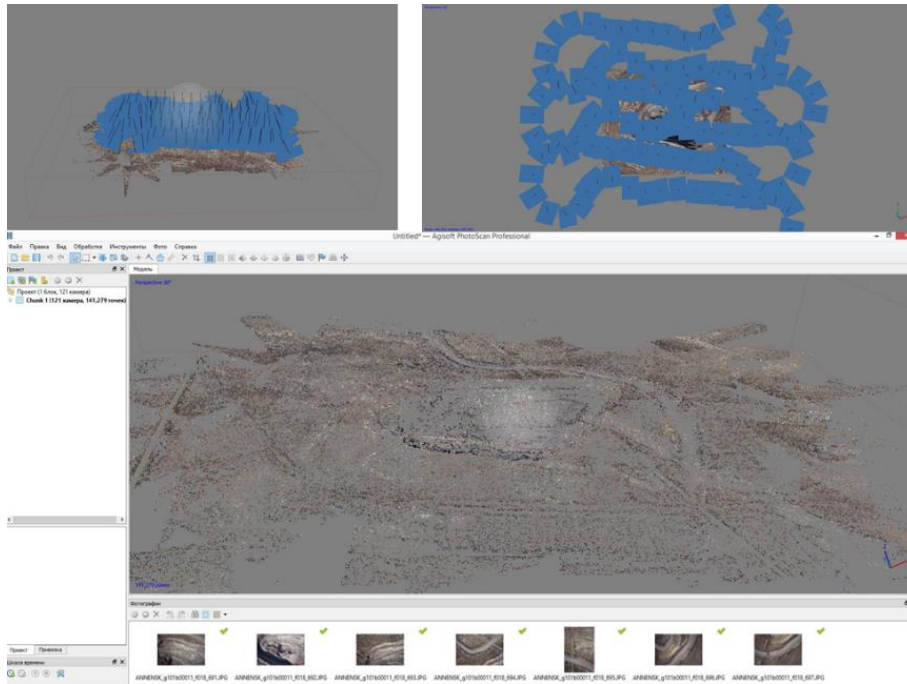
Figure 2 – The process of building a point cloud for polygon photogrammetry in Agisoft PhotoScan

The process of creating a model for marker detection involves processing the point cloud, which is a time-consuming task. However, the output is a model of high quality that can be used to detect markers. These markers, which are placed on the boundary of the area being defined, contain the initial coordinates of reference points. In the field, these reference points are determined at the survey site by marking. The markers can take the form of a "+" mark, such as a plus sign, which is easily visible in an aerial survey, or an object with a clear center, as shown in Figure 3.
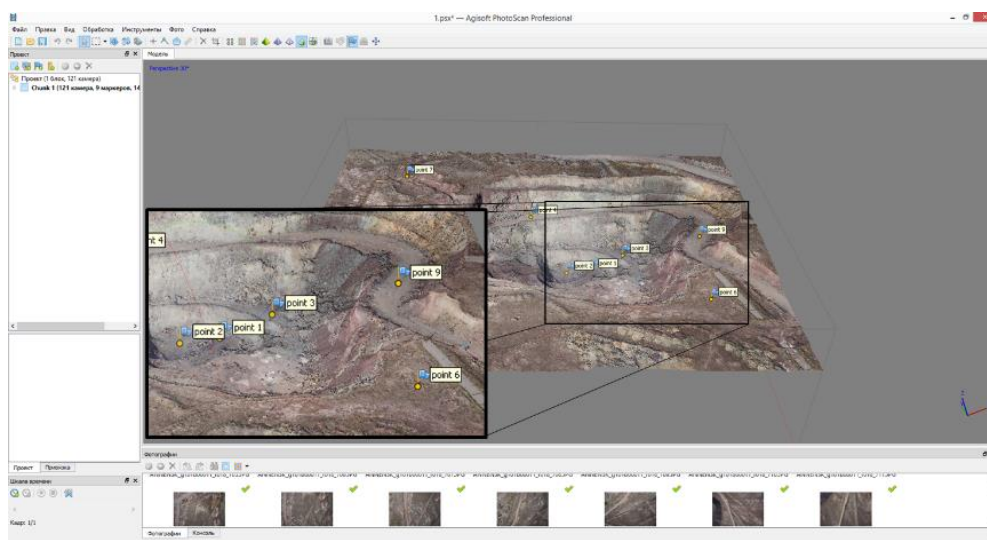
Figure 3 – Identification of markers on the territory of the polygon in the Agisoft PhotoScan environment

3. Results and Discussion

After comparing traditional and automated methods of determining ground coordinates, it was discovered that there were notable discrepancies in both the final values and the time taken to determine coordinate points. Previous research exploring comparative deviation analysis, focused on creating point clouds via laser and digital photogrammetry, is discussed in [9]. The accuracy of point positioning by computer programs is analyzed in [10], where the coordinates of points obtained through tachymetric survey are used as the reference system by the authors.

Figure 4 below shows the model subjected to linear transformations.
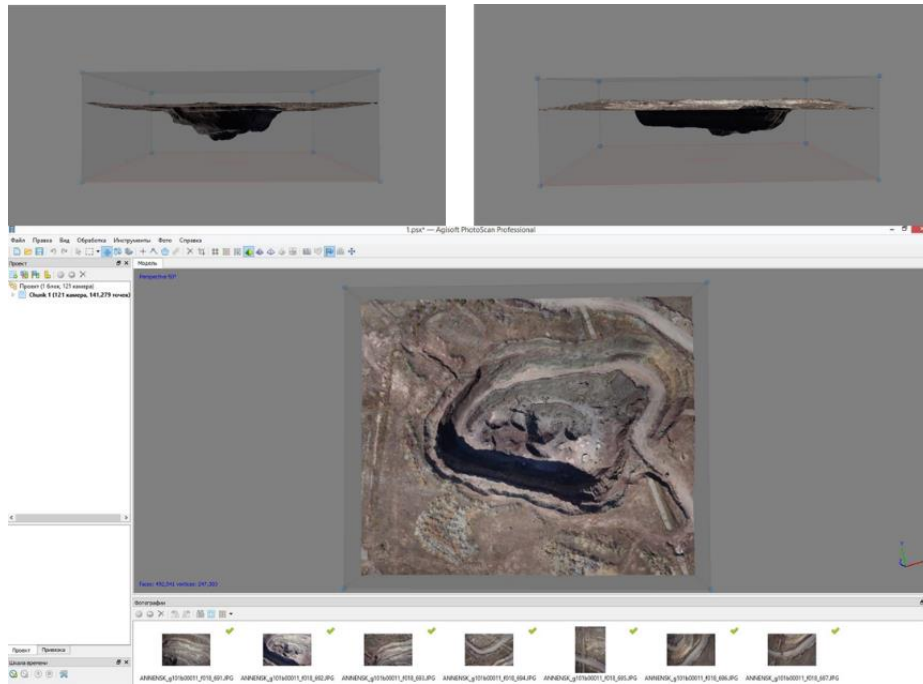
Figure 4 – Building a vertical leveling profile in Agisoft PhotoScan according to markers

The similarity transformation model is derived from 7 parameters: 3 translation parameters, 3 rotation parameters, 1 stretching and compression parameter). This approach solves only linear distortions while nonlinear distortions which are also present in the model can be the reason for further errors in the model georeferencing and calculations. To reduce influence of nonlinear distortions markers or reference points with known coordinates were used.

Table 1 below shows the deviation between traditional point coordinates (X1, Y1, Z1) and automated (X2, Y2, Z2) methods in Agisoft PhotoScan.

Table 1 – Deviation of coordinates

№	X1	X2	Xdiff	Incl%	Y1	Y2	Ydiff	Incl%	Z1	Z2	Zdiff	Incl%
1	47.8771	48.8834	1.0063	2.10%	67.5170	68.5548	1.0378	1.54%	356.9000	357.9265	1.0265	0.29%
2	47.8771	48.9085	1.0314	2.15%	67.5170	67.5309	0.0139	0.02%	357.2000	357.2502	0.0502	0.01%
3	47.8771	48.8904	1.0133	2.12%	67.5170	67.5378	0.0209	0.03%	356.5000	356.5235	0.0235	0.01%
4	47.8771	47.9010	0.0240	0.05%	67.5170	67.5509	0.0339	0.05%	356.7000	356.7276	0.0276	0.01%
5	47.8771	47.9171	0.0400	0.08%	67.5170	67.5235	0.0065	0.01%	356.2000	357,2477	1,0477	0,29%
6	47,8771	47,8840	0,0069	0,01%	67,5170	67,5432	0,0262	0.04%	357.0000	357.0320	0.0320	0.01%
7	47.8771	47.9259	0.0488	0.10%	67.5170	68.5227	1.0057	1.49%	356.3000	356.3364	0.0364	0.01%
8	47.8771	47.9240	0.0470	0.10%	67.5170	67.5344	0.0174	0.03%	356.8000	357.8267	1.0267	0.29%
9	47.8771	48.9218	1.0447	2.18%	67.5170	67.5628	0.0458	0.07%	356.6000	357.6500	1.0500	0.29%
10	47.8771	48.8881	1.0110	2.11%	67.5170	67.5474	0.0303	0.04%	357.2000	357.2447	0.0447	0.01%

11	47.8771	47.8801	0.0031	0.01%	67.5170	67.5482	0.0312	0.05%	356.9000	356.9422	0.0422	0.01%
12	47.8771	48.8946	1.0175	2.13%	67.5170	67.5557	0.0387	0.06%	356.9000	356.9248	0.0248	0.01%
13	47.8771	47.9170	0.0399	0.08%	67.5170	67.5515	0.0345	0.05%	356.9000	356.9343	0.0343	0.01%
14	47.8771	48.9023	1.0252	2.14%	67.5170	67.5509	0.0339	0.05%	357.2000	358.2510	1.0510	0.29%
15	47.8817	48.9001	1.0185	2.13%	67.5212	67.5470	0.0258	0.04%	517.7000	519.7231	2.0231	0.39%
16	47.8818	47.8932	0.0115	0.02%	67.5205	67.5551	0.0346	0.05%	513.8000	513.8261	0.0261	0.01%
17	47.8815	47.9037	0.0222	0.05%	67.5198	68.5253	1.0055	1.49%	514.1000	514.1107	0.0107	0.00%
18	47.8812	47.9295	0.0483	0.10%	67.5192	68.5481	1.0288	1.52%	519.1000	519.1238	0.0238	0.00%
19	47.8810	47.9173	0.0363	0.08%	67.5187	68.5557	1.0370	1.54%	523.0000	524.0058	1.0058	0.19%
20	47.8809	47.8956	0.0147	0.03%	67.5181	67.5601	0.0420	0.06%	519.7000	520.7050	1.0050	0.19%
21	47.8809	47.8950	0.0140	0.03%	67.5175	67.5570	0.0395	0.06%	514.3000	514.3113	0.0113	0.00%
22	47.8810	47.8855	0.0045	0.01%	67.5168	67.5617	0.0448	0.07%	515.5000	515.5459	0.0459	0.01%
23	47.8810	47.8849	0.0039	0.01%	67.5162	68.5228	1.0066	1.49%	516.3000	517.3044	1.0044	0.19%
24	47.8809	48.9207	1.0397	2.17%	67.5156	67.5662	0.0506	0.07%	514.6000	515.6264	1.0264	0.20%
25	47.8809	47.9215	0.0406	0.08%	67.5150	67.5656	0.0507	0.08%	514.9000	514.9234	0.0234	0.00%
26	47.8809	48.8988	1.0179	2.13%	67.5144	67.5491	0.0348	0.05%	516.2000	517.2142	1.0142	0.20%
27	47.8808	48.9199	1.0391	2.17%	67.5138	67.5177	0.0039	0.01%	518.9000	518.9173	0.0173	0.00%
28	47.8805	47.8847	0.0042	0.01%	67.5132	68.5253	1.0121	1.50%	518.1000	520.1299	2.0299	0.39%
29	47.8801	47.9012	0.0211	0.04%	67.5130	67.5457	0.0327	0.05%	514.1000	515.1421	1.0421	0.20%
30	47.8797	48.9117	1.0320	2.16%	67.5130	67.5453	0.0323	0.05%	511.4000	511.4121	0.0121	0.00%
31	47.8793	47.9150	0.0356	0.07%	67.5134	67.5615	0.0481	0.07%	510.1000	511.1148	1.0148	0.20%
32	47.8792	48.8821	1.0028	2.09%	67.5140	67.5262	0.0122	0.02%	509.0000	510.0468	1.0468	0.21%
33	47.8795	47.8830	0.0036	0.01%	67.5145	67.5199	0.0055	0.01%	507.8000	508.8086	1.0086	0.20%
34	47.8798	48.8924	1.0126	2.11%	67.5148	67.5628	0.0480	0.07%	511.4000	511.4267	0.0267	0.01%
35	47.8800	48.9268	1.0468	2.19%	67.5151	68.5507	1.0356	1.53%	517.0000	517.0330	0.0330	0.01%
36	47.8802	47.8893	0.0091	0.02%	67.5157	68.5276	1.0120	1.50%	519.6000	519.6370	0.0370	0.01%
37	47.8801	47.9178	0.0377	0.08%	67.5163	68.5386	1.0223	1.51%	514.1000	516.1508	2.0508	0.40%
38	47.8800	47.8879	0.0079	0.02%	67.5169	67.5306	0.0136	0.02%	517.6000	518.6193	1.0193	0.20%
39	47.8800	47.9297	0.0497	0.10%	67.5175	67.5415	0.0239	0.04%	518.2000	518.2295	0.0295	0.01%
40	47.8800	47.8880	0.0079	0.02%	67.5181	67.5552	0.0371	0.05%	519.5000	520.5162	1.0162	0.20%
41	47.8801	47.9212	0.0412	0.09%	67.5188	67.5326	0.0138	0.02%	523.0000	524.0091	1.0091	0.19%
42	47.8801	47.9189	0.0389	0.08%	67.5194	68.5565	1.0371	1.54%	525.1000	526.1468	1.0468	0.20%
43	47.8801	47.8880	0.0079	0.02%	67.5200	67.5338	0.0138	0.02%	522.3000	522.3347	0.0347	0.01%
44	47.8801	48.9036	1.0235	2.14%	67.5207	67.5462	0.0255	0.04%	519.1000	519.1506	0.0506	0.01%
45	47.8801	47.8925	0.0124	0.03%	67.5214	68.5583	1.0369	1.54%	523.5000	523.5495	0.0495	0.01%
46	47.8801	47.8932	0.0131	0.03%	67.5220	68.5394	1.0174	1.51%	525.1000	526.1498	1.0498	0.20%
47	47.8800	47.8933	0.0134	0.03%	67.5227	67.5401	0.0174	0.03%	526.8000	527.8038	1.0038	0.19%
48	47.8797	48.8975	1.0178	2.13%	67.5231	68.5328	1.0097	1.50%	526.1000	526.1165	0.0165	0.00%
49	47.8792	47.8908	0.0115	0.02%	67.5232	67.5451	0.0219	0.03%	522.4000	522.4164	0.0164	0.00%
50	47.8788	47.9000	0.0212	0.04%	67.5229	67.5335	0.0106	0.02%	518.5000	518.5383	0.0383	0.01%
51	47.8787	48.9074	1.0287	2.15%	67.5223	67.5487	0.0264	0.04%	515.4000	516.4364	1.0364	0.20%
52	47.8789	47.9252	0.0464	0.10%	67.5217	67.5382	0.0165	0.02%	513.9000	514.9192	1.0192	0.20%
53	47.8791	48.9035	1.0244	2.14%	67.5212	67.5285	0.0072	0.01%	518.8000	519.8361	1.0361	0.20%
54	47.8793	48.8923	1.0130	2.12%	67.5208	67.5703	0.0495	0.07%	527.0000	528.0124	1.0124	0.19%
55	47.8794	48.9292	1.0498	2.19%	67.5202	68.5319	1.0117	1.50%	523.8000	523.8103	0.0103	0.00%
56	47.8793	47.9194	0.0401	0.08%	67.5195	67.5540	0.0345	0.05%	521.2000	522.2282	1.0282	0.20%
57	47.8793	47.9292	0.0499	0.10%	67.5188	68.5230	1.0041	1.49%	524.0000	524.0398	0.0398	0.01%
58	47.8793	47.8832	0.0039	0.01%	67.5181	67.5221	0.0040	0.01%	525.2000	528.2248	3.0248	0.58%

59	47.8793	47.9169	0.0376	0.08%	67.5174	67.5514	0.0340	0.05%	522.9000	523.9322	1.0322	0.20%
60	47.8793	47.9067	0.0274	0.06%	67.5168	67.5470	0.0303	0.04%	521.4000	521.4080	0.0080	0.00%
61	47.8793	47.8961	0.0168	0.04%	67.5161	67.5236	0.0076	0.01%	522.6000	523.6199	1.0199	0.20%
62	47.8793	48.8959	1.0166	2.12%	67.5155	68.5212	1.0058	1.49%	523.8000	524.8058	1.0058	0.19%
63	47.8793	47.8951	0.0158	0.03%	67.5148	67.5374	0.0226	0.03%	523.1000	523.1313	0.0313	0.01%
64	47.8793	47.9154	0.0361	0.08%	67.5142	67.5367	0.0225	0.03%	521.9000	521.9084	0.0084	0.00%
65	47.8792	47.8827	0.0035	0.01%	67.5135	67.5402	0.0267	0.04%	521.1000	522.1182	1.0182	0.20%
66	47.8788	47.8903	0.0115	0.02%	67.5130	67.5183	0.0052	0.01%	518.9000	518.9364	0.0364	0.01%
67	47.8784	48.8870	1.0086	2.11%	67.5128	68.5520	1.0392	1.54%	514.7000	515.7388	1.0388	0.20%
68	47.8779	49.9242	2.0463	4.27%	67.5130	67.5605	0.0476	0.07%	509.7000	510.7340	1.0340	0.20%
69	47.8777	48.9171	1.0395	2.17%	67.5134	68.5548	1.0414	1.54%	505.8000	506.8484	1.0484	0.21%
70	47.8776	48.8997	1.0221	2.13%	67.5140	67.5509	0.0369	0.05%	504.3000	504.3095	0.0095	0.00%
71	47.8779	47.8896	0.0117	0.02%	67.5144	67.5550	0.0406	0.06%	505.0000	505.0104	0.0104	0.00%
72	47.8782	47.9158	0.0376	0.08%	67.5147	67.5396	0.0249	0.04%	511.2000	513.2402	2.0402	0.40%
73	47.8785	48.8962	1.0177	2.13%	67.5151	67.5195	0.0044	0.01%	516.5000	517.5420	1.0420	0.20%
74	47.8786	47.8837	0.0051	0.01%	67.5156	68.5368	1.0212	1.51%	515.8000	515.8089	0.0089	0.00%
75	47.8785	48.8996	1.0211	2.13%	67.5163	67.5403	0.0240	0.04%	513.9000	514.9069	1.0069	0.20%
76	47.8784	47.9091	0.0307	0.06%	67.5169	67.5538	0.0369	0.05%	517.1000	517.1283	0.0283	0.01%
77	47.8784	48.8963	1.0179	2.13%	67.5174	68.5362	1.0188	1.51%	518.0000	518.0403	0.0403	0.01%
78	47.8785	47.8952	0.0167	0.03%	67.5180	67.5225	0.0045	0.01%	517.3000	517.3493	0.0493	0.01%
79	47.8785	47.8878	0.0093	0.02%	67.5186	68.5608	1.0422	1.54%	519.9000	519.9151	0.0151	0.00%
80	47.8785	48.9018	1.0234	2.14%	67.5193	68.5669	1.0476	1.55%	515.5000	515.5244	0.0244	0.00%
81	47.8784	48.8978	1.0194	2.13%	67.5200	67.5333	0.0133	0.02%	516.3000	517.3090	1.0090	0.20%
82	47.8785	47.8816	0.0031	0.01%	67.5206	68.5364	1.0158	1.50%	520.0000	522.0214	2.0214	0.39%
83	47.8785	48.9266	1.0482	2.19%	67.5212	68.5350	1.0138	1.50%	521.4000	521.4258	0.0258	0.00%
84	47.8785	47.9192	0.0407	0.09%	67.5218	67.5366	0.0148	0.02%	520.1000	520.1106	0.0106	0.00%
85	47.8784	47.9140	0.0356	0.07%	67.5224	67.5578	0.0354	0.05%	519.9000	519.9459	0.0459	0.01%
86	47.8781	47.8990	0.0209	0.04%	67.5228	67.5277	0.0049	0.01%	516.9000	517.9433	1.0433	0.20%
87	47.8777	47.8979	0.0202	0.04%	67.5228	67.5567	0.0339	0.05%	507.9000	508.9377	1.0377	0.20%
88	47.8773	47.9068	0.0295	0.06%	67.5224	68.5406	1.0182	1.51%	504.7000	505.7085	1.0085	0.20%
89	47.8773	47.9063	0.0290	0.06%	67.5218	67.5608	0.0390	0.06%	509.0000	509.0043	0.0043	0.00%
90	47.8774	47.9283	0.0508	0.11%	67.5212	67.5248	0.0036	0.01%	509.5000	510.5238	1.0238	0.20%
91	47.8776	47.9033	0.0257	0.05%	67.5207	67.5596	0.0389	0.06%	513.8000	513.8052	0.0052	0.00%
92	47.8777	48.9081	1.0304	2.15%	67.5201	67.5565	0.0364	0.05%	519.0000	520.0415	1.0415	0.20%
93	47.8777	47.8878	0.0101	0.02%	67.5195	67.5222	0.0027	0.00%	518.5000	518.5161	0.0161	0.00%
94	47.8777	47.8822	0.0046	0.01%	67.5189	67.5265	0.0076	0.01%	520.3000	521.3109	1.0109	0.19%
95	47.8777	47.8957	0.0180	0.04%	67.5182	67.5389	0.0206	0.03%	521.5000	521.5281	0.0281	0.01%
96	47.8777	47.8909	0.0132	0.03%	67.5176	68.5394	1.0217	1.51%	519.9000	520.9314	1.0314	0.20%
97	47.8777	47.9227	0.0450	0.09%	67.5170	68.5631	1.0461	1.55%	517.7000	517.7328	0.0328	0.01%
98	47.8777	47.9290	0.0512	0.11%	67.5163	67.5333	0.0169	0.03%	517.7000	518.7373	1.0373	0.20%
99	47.8777	48.8983	1.0205	2.13%	67.5157	67.5269	0.0111	0.02%	518.8000	519.8412	1.0412	0.20%
100	47.8777	48.9057	1.0280	2.15%	67.5151	67.5465	0.0314	0.05%	517.6000	517.6168	0.0168	0.00%
101	47.8777	47.9001	0.0224	0.05%	67.5145	67.5375	0.0230	0.03%	517.0000	517.0477	0.0477	0.01%
102	47.8776	48.8898	1.0122	2.11%	67.5139	67.5614	0.0475	0.07%	515.3000	515.3031	0.0031	0.00%
103	47.8773	47.8843	0.0070	0.01%	67.5133	67.5586	0.0452	0.07%	511.2000	511.2159	0.0159	0.00%
104	47.8769	48.8985	1.0216	2.13%	67.5131	67.5240	0.0110	0.02%	506.2000	506.2144	0.0144	0.00%
105	47.8764	49.8932	2.0168	4.21%	67.5132	67.5250	0.0118	0.02%	504.8000	504.8493	0.0493	0.01%
106	47.8761	48.9068	1.0307	2.15%	67.5137	67.5602	0.0465	0.07%	504.7000	504.7240	0.0240	0.00%

107	47.8760	48.9202	1.0442	2.18%	67.5143	67.5414	0.0271	0.04%	504.8000	505.8174	1.0174	0.20%
108	47.8762	48.8832	1.0069	2.10%	67.5148	68.5347	1.0200	1.51%	506.0000	507.0223	1.0223	0.20%
109	47.8765	48.8858	1.0092	2.11%	67.5151	68.5238	1.0087	1.49%	509.3000	510.3066	1.0066	0.20%
110	47.8768	47.8932	0.0164	0.03%	67.5155	67.5433	0.0278	0.04%	514.3000	514.3387	0.0387	0.01%
111	47.8769	47.8948	0.0179	0.04%	67.5160	68.5544	1.0384	1.54%	513.6000	513.6049	0.0049	0.00%
112	47.8768	47.8995	0.0227	0.05%	67.5166	67.5477	0.0310	0.05%	512.2000	513.2256	1.0256	0.20%
113	47.8768	47.9158	0.0391	0.08%	67.5172	68.5326	1.0154	1.50%	514.7000	515.7281	1.0281	0.20%
114	47.8768	47.9087	0.0319	0.07%	67.5179	68.5479	1.0300	1.53%	513.7000	513.7311	0.0311	0.01%
115	47.8769	47.8816	0.0048	0.01%	67.5185	67.5247	0.0061	0.01%	513.8000	513.8040	0.0040	0.00%
116	47.8769	48.9042	1.0273	2.15%	67.5192	68.5669	1.0477	1.55%	516.3000	516.3253	0.0253	0.00%
117	47.8769	49.8816	2.0047	4.19%	67.5198	67.5407	0.0209	0.03%	516.9000	517.9249	1.0249	0.20%
118	47.8769	47.9025	0.0257	0.05%	67.5204	67.5297	0.0093	0.01%	517.9000	518.9306	1.0306	0.20%
119	47.8769	47.8811	0.0042	0.01%	67.5210	67.5444	0.0234	0.03%	516.6000	516.6403	0.0403	0.01%
120	47.8769	48.8822	1.0053	2.10%	67.5216	67.5660	0.0444	0.07%	512.4000	514.4281	2.0281	0.40%
121	47.8768	47.9244	0.0475	0.10%	67.5221	67.5611	0.0389	0.06%	514.2000	514.2438	0.0438	0.01%
122	47.8766	47.9217	0.0450	0.09%	67.5226	67.5420	0.0194	0.03%	513.5000	514.5417	1.0417	0.20%
	Average deviation		0.87%				0.45%					0.12%

The Agisoft PhotoScan software capability was evaluated based on a comparison of the data obtained with the Leica TSO06 total station. As noted earlier, the instrument itself has a level of tolerance (Figure 1), so it is worth paying attention to the smallest and largest values. This problem is extensively discussed in [11], where the object of the study is a specific building with right angles and a flat surface. In our case, the ground, which forms the relief of the object on which the survey was carried out, gives a large error, which is visually reflected in the table above. Minimal error in X-axis was 0.0031, in Y-axis 0.0027 and in Z-axis 0.0031 degrees. Maximum values for X axis was 2.0463, Y axis 1.0477 and Z axis 3.0248 degrees. As expected earlier in the construction of points in the plane difficulties were caused by the triangulation angle, because the scheme of building depends on the geometry of the object, which has no clear reference points in nature. At all this sighting error has a higher priority than instrumental origin and ranges between ±0.3-0.4" in first-class work and ±1" in networks of crowding, which is worth considering when surveying [12]. Similar measurements to confirm the allowable errors were carried out in the article [13] , where the relative error was less than 10%, which corresponds to the real field data. The use of non-metric cameras is quite a serious step for photogravimetry, but correctly chosen software allows to minimize the error range.

A color-coded system was used to indicate the level of difference between the known and obtained coordinates, with green, yellow, and red signifying minimally acceptable, not significant, and maximum critical differences, respectively. The average deviation between the known and Agisoft PhotoScan coordinates was 0.87% in the X-axis, 0.45% in the Y-axis, and 0.12% in the Z-axis. The total station survey took approximately two days to complete for all 122 points, while finding the remaining 121 points only took about three hours due to the process being automated. It should be noted that the time spent working with the software can also be reduced by using a more powerful computer to process the data received from the aircraft.

4. Conclusions

The authors of the article conducted a comparative analysis between traditional and automated processes for determining surveying coordinates. Based on the results of the study, the following conclusions were made:

1. The traditional method allowed for a quick visual estimation of the survey area.

2. The traditional method also allowed for the consideration of terrain peculiarities and existing objects.

3. The automated method provided visualization of the current situation on the construction site.

4. The automated method allowed for an automatic process of coordinate determination using one initial point obtained with a total station.

5. The study revealed some level of inaccuracy in coordinate values when comparing data obtained from the total station and the software.

References

1. Efficiency optimization and quality control of engineering geodesy processes in civil engineering / V. Berkhahn, F. Berner, H. Kutterer, V. Schwieger, J. Hirschner, I. Rehr, N. Rinke, J. Schweitzer // BAUINGENIEUR. — 2010. — Vol. 85. — P. 491–501.
2. UAS Point Cloud Accuracy Assessment Using Structure from Motion–Based Photogrammetry and PPK Georeferencing Technique for Building Surveying Applications / J.G. Martinez, G. Albeaino, M. Gheisari, W. Volkmann, L.F. Alarcón // Journal of Computing in Civil Engineering. — 2021. — Vol. 35, No. 1. — P. 05020004. https://doi.org/10.1061/(ASCE)CP.1943-5487.0000936
3. Web-Based Architecture for Automating Quantity Surveying Construction Cost Calculation / J.H. Yousif, S. N. Abdul Majeed, F. J. I. Al Azzawi // Infrastructures. — 2020. — Vol. 5, No. 6. — P. 45. https://doi.org/10.3390/infrastructures5060045
4. Geometric accuracy investigations of terrestrial laser scanner systems in the laboratory and in the field / T.P. Kersten, M. Lindstaedt // Applied Geomatics. — 2022. — Vol. 14, No. 2. — P. 421–434. https://doi.org/10.1007/s12518-022-00442-2
5. Assessing the Accuracy of High Resolution Digital Surface Models Computed by PhotoScan® and MicMac® in Sub-Optimal Survey Conditions / M. Jaud, S. Passot, R. Le Bivic, C. Delacourt, P. Grandjean, N. Le Dantec // Remote Sensing. — 2016. — Vol. 8, No. 6. — P. 465. https://doi.org/10.3390/rs8060465
6. Structure from motion processing of analogue images captured by rollei metric camera, digitized with various scanning resolution / A. Dlesk, K. Vach, K. Pavelka // Acta Polytechnica. — 2020. — Vol. 60, No. 4. — P. 288–302. https://doi.org/10.14311/AP.2020.60.0288
7. Assessing the performance of commercial Agisoft PhotoScan software to deliver reliable data for accurate3D modelling / A. Jebur, F. Abed, M. Mohammed // MATEC Web of Conferences. — 2018. — Vol. 162. — P. 03022. https://doi.org/10.1051/matecconf/201816203022
8. Performance comparison analysis of 3D reconstruction modeling software in construction site visualization and mapping / A. Keyvanfar, A. Shafaghat, M.S. Rosley // International Journal of Architectural Computing. — 2022. — Vol. 20, No. 2. — P. 453–475. https://doi.org/10.1177/14780771211066876
9. A comparative study between photogrammetry and laser technology applied on model turbine blades / D. Nedelcu, G.R. Gillich, A. Gerocs, I. Padurean // Journal of Physics: Conference Series. — 2020. — Vol. 1426, No. 1. — P. 012026. https://doi.org/10.1088/1742-6596/1426/1/012026
10. The analysis of the accuracy of spatial models using photogrammetric software: Agisoft Photoscan and Pix4D / A. Barbasiewicz, T. Widerski, K. Daliga // E3S Web of Conferences. — 2018. — Vol. 26. — P. 00012. https://doi.org/10.1051/e3sconf/20182600012
11. Assessing the performance of commercial Agisoft PhotoScan software to deliver reliable data for accurate3D modelling [Текст] / A. Jebur, F. Abed, M. Mohammed // MATEC Web of Conferences. — 2018. — Т. 162. — С. 03022. https://doi.org/10.1051/matecconf/201816203022
12. Evaluation of Stereo Matching Algorithms and Dynamic Programming for 3D Triangulation / T.C. Huat, N.A. Manap // Advanced Computer and Communication Engineering Technology: Vol. 315: Lecture Notes in Electrical Engineering. — Cham: Springer International Publishing, 2015. — P. 641–650. https://doi.org/10.1007/978-3-319-07674-4_60
13. Construction and Accuracy Test of a 3D Model of Non-Metric Camera Images Using Agisoft PhotoScan / X. quan Li, Z. an Chen, L. ting Zhang, D. Jia // Procedia Environmental Sciences. — 2016. — Vol. 36. — P. 184–190. https://doi.org/10.1016/j.proenv.2016.09.031

Information about authors:
Zhassulan Kuzbakhov – MSc Student, Department of Civil Engineering, L.N. Gumilyov Eurasian National University, Astana, Kazakhstan, zhaaas0613@gmail.com
Shyngys Zharassov – PhD Student, Department of Civil Engineering, L.N. Gumilyov Eurasian National University, Astana, Kazakhstan, zhshzh95@gmail.com

Author Contributions:
Zhassulan Kuzbakhov – concept, methodology, resources, analysis, editing, funding acquisition.
Shyngys Zharassov – data collection, modeling, testing, visualization, interpretation, drafting.

Article

Exploring the capabilities of 3D Printer S-6045 for additive manufacturing of street furniture

Gulnaz Zhairbaeva*, Zulfiya Aubakirova, Yana Ivashina, Alexandr Soldun,
Alina Makienko[5]

School of Architecture and Construction, D. Serikbayev East Kazakhstan Technical University, Ust-Kamenogorsk, Kazakhstan
*Correspondence: gulnaz.w@mail.ru

Abstract. This paper examines the potential of 3D printing for additive manufacturing of street furniture, specifically a flowerbed measuring 1.63 m in length, 0.3 m in height according to a custom design. The study investigates the production process, material selection, and design considerations for street furniture, as well as the workability of the selected concrete mixture and the strength of the hardened structure. It uses the S-6045 3D printer to produce the flowerbed and tests the concrete mixtures for workability and strength of concrete at the age of 28 days. The study produced a concrete mixture that exhibits the required attributes for use with the S-6045 3D printer. The findings may also have implications for other applications of additive manufacturing in the urban environment.
Keywords: additive manufacturing, street furniture, concrete mixtures, workability, strength.

1. Introduction

Today, additive building technology is becoming more and more popular. The use of 3D printing in construction is due to the expectations of unlimited design of forms and elements, as well as the provision of new aesthetic and their functional characteristics [1]. The development of additive technologies is due to many factors: increasing the level of automation, improving product quality, reducing construction time, reducing the amount of waste in the production process. These factors stimulate interest in additive technologies in construction, and allow the use of 3D - prototyping as an alternative to traditional construction methods [2]. The commercial success of 3D printing lies in the creation of robust design and manufacturing processes, and in the ability of architects and engineers to develop certified construction materials and components [3].

Also additive manufacturing is a rapidly developing technology with a wide range of applications in various fields. One of the areas where it has gained significant interest is street furniture. Street furniture refers to the items that enhance the functionality and aesthetics of public spaces, including parks, sidewalks, and urban plazas. Examples of street furniture include benches, trash cans, bus stops, bike racks, and streetlights [4].

Additive manufacturing has several advantages and disadvantages for street furniture production. While it offers greater design flexibility, faster production times, reduced material waste, and customization options, it may also be expensive, have limited production sizes, require additional finishing steps, have material limitations, and may not be as durable as traditionally manufactured street furniture. Ultimately, the decision to use 3D printing for street furniture production will depend on the specific needs of a project and the balance of advantages and disadvantages for that particular situation [5].

There are several 3D printers available on the market that can be used for additive manufacturing of street furniture, and one of them is 3D printer S-6045 [6]. S-6045 is a professional-grade additive manufacturing system that offers a large build volume, high accuracy, and excellent material compatibility. It is capable of producing high-quality parts with a variety of materials, including thermoplastics, composites, and metals.

The aim of this study is to explore the capabilities of the S-6045 3D printer for additive manufacturing of street furniture, in particular the flowerbed of cutom design. We investigated the production process, material selection, and design considerations for street furniture. Additionally, we evaluated the workability of the selected mixture, as well as the strength of hardened structure.

The results of this study may provide insights into the potential of 3D printing for street furniture production and inform the design and manufacturing practices for this field. The findings may also have implications for other applications of additive manufacturing in the urban environment.

Objectives of the study:
- Investigating the parameters of 3D printer;
- Selecting the concrete mixtures components;
- Testing concrete mixtures for workability and early strength;
- Designing the structure and setting parameters for 3D printing;
- 3D printing, reinforcing and filling voids with heavy concrete.

2. Methods

A 3D printer S-6045 from D. Serikbayev East Kazakhstan technical university was used in this study. The S-6045 is a modern construction printer belonging to the category of professional laboratory equipment. Its characteristics are presented in Table 1 below.

Table 1 – S-6045 characteristics [6]

Parameter	Value
Manufacturer	AMT Group of Companies, Russia, Yaroslavl
Type of drive	Stepper motors with cylindrical gears
Productivity, m³/h	0.7
Working area, m	3.5×3.1×1.0
Components	Printer, laptop with a set of licensed software, control cabinet, passport, operation manual, non-return transport packaging, high pressure washer, manual mixer, three additional nozzles of different diameters.
Positioning speed, m/mm	12
Positioning accuracy, mm	2
Power consumption, kW	2.4
Size of the printed layer (height, width), mm	5-10, 20-50
Concrete consumption, m³ per 1 m² of wall with 4-layer printing	0.12
Dimensions (length, width, height)	4.0×5.0×3.6
Weight, kg	870
Types of mixtures	Cement mixtures with or without plasticizers and antifreeze additives, gypsum mixtures
Requirements for operating conditions	The equipment must be operated in dry, enclosed heated rooms at operating temperatures from +5 °C to +40 °C and at a humidity of no more than 60 %, non-condensing

Two concrete compositions had to be prepared for the production of the intended structure: for additive printing and for filling the voids. The water according to [7] in the ratio of 0.18 l per 1 kg of dry material (cement and sand), cement according to [8] at a water-cement ratio of 1/3, sand with a fraction of 2.5 mm according to [9], and plasticizers according to [10] were selected for the mixture to additive printing. To fill the voids, the same components were supplemented with coarse aggregate (crushed stone) by [11] in a ratio of 1/3 with cement, in order to obtain heavy concrete.

The composition for additive printing was subjected to tests for workability at a mixture state and for compressive strength at a hardened state.

The workability tests were conducted according to [12]. According to this standard, the workability of a concrete mixture is evaluated by measuring the depth of immersion of a reference cone in the mixture, expressed in millimeters. The cone should immerse freely in the mixture. The second reading is taken 1 minute after the start of immersion of the cone. The immersion depth of the cone, measured with an error of up to 1 mm, is determined as the difference between the first and the second reading. At least three samples of the mixture are tested, the average results of which should not exceed 20 mm.

The compressive strength tests were conducted according to [13] using hydraulic press. Two specimens were taken for the test, extracted from a structure printed in 6 layers and cured for 28 days, with different surface areas (i.e., footprints).

A street flowerbed custom design was selected for printing with the dimensions of 1.63 m in length, 0.3 m in height. It was designed using AutoCAD as a continuous closed-loop polyline, converted to 3D using SheetCam and integrated to the Mach3 software coming with S-6045. The following 3D printing parameters were set in Mach3 preliminarily:

- The average printing speed of 0.5 m^3/h
- The working area was 2 m^2, which is slightly larger than the size of the printed structure;
- The coordinates of a starting point, where each layer closes the printing layer and goes to the next layer;
- The height of one layer is 10 mm and the width of the layer is 35 mm.

The 3D printing of the intended structure was performed in steps to the height of 0.3 m, each containing certain layers, enabling the fresh concrete to gain a certain level of strength, at which it can carry the subsequent layers. During printing it was another task to define an optimal mode of printing for a chosen concrete composition (dependence between the number of simultaneously printed layers, printing speed, layer height and width, as well as a curing time).

After the structure was printed, its inner void was reinforced with a knitted frame made of rebar with a diameter of 8 mm and poured by heavy concrete.

3. Results and Discussion

The results of workability test of the printing mixture is presented in Figure 1 below.
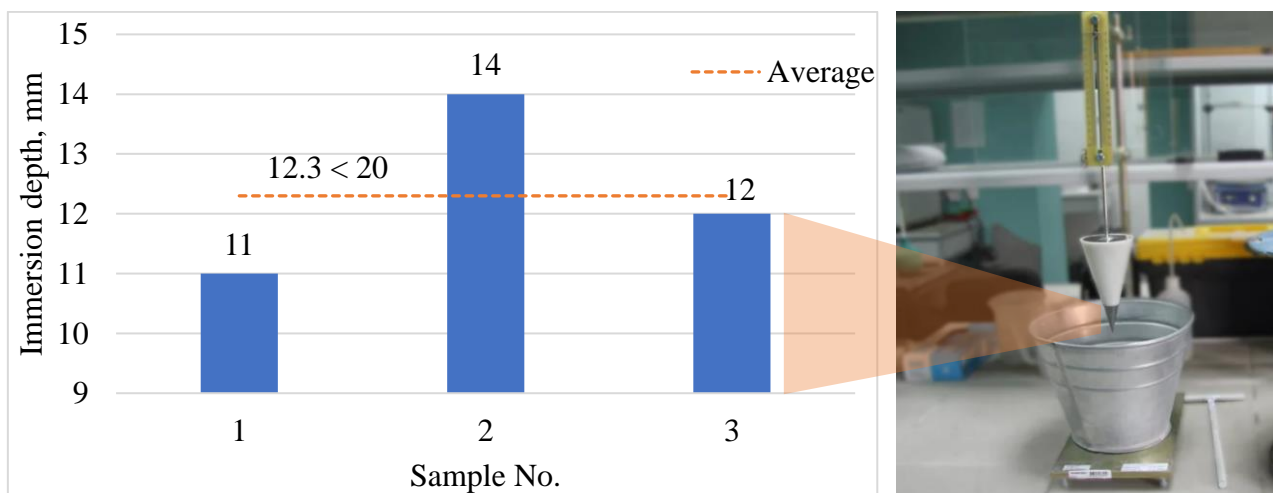

Figure 1 – Workability test results

The figure above shows that the measurement of cone immersion depths amounted 11, 14 and 12 mm for the samples 1, 2 and 3 respectively. Their average value is 12.3 mm, which is less than 20 mm. Consequently, the selected composition meets the requirements for workability specified in [12].

After the workability test, the prepared mixture was filled into the mortar hopper and the 3D printer was put into operation. As planned, 6 layers of the structure were printed, of which after 28 days of curing, 2 samples were extracted for strength testing with surface areas of 54.6 and 46 cm2 respectively. The results of strength test are presented in Figure 2 below.
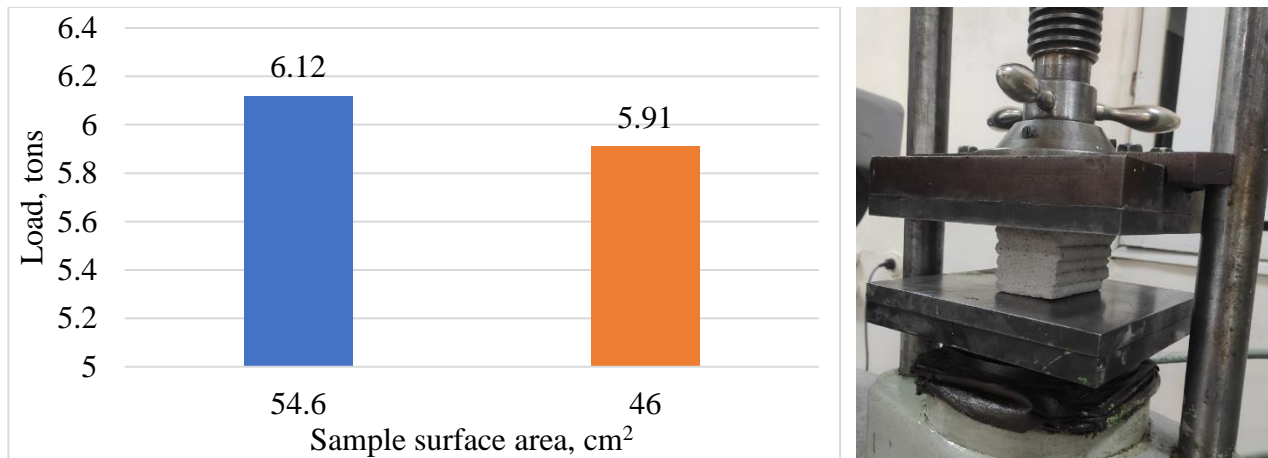
Figure 2 – Compression test results

The compression test showed that the two samples crashed at the loads of 6.12 and 5.91 tons respectively. Taking into account their surface area, it can be assumed that both samples showed the similar compressive strength of around 10 MPa. This value corresponds to the concrete grade of M100 according to [14]. Accordin to this standard, concretes of grade M100 can be used for small repairs or as a permanent formwork for which it is necessary to pour heavier concrete.

After the compression test, the 3D printing of the intended structure started. The first trial of simultaneous printing ended with 14 layers then fall. This led to the number of layers to be decreased to 12 at the second trial. The second trial did not fall, but slightly bended. This could be due to the vibration of printing aggregate while moving, as well as viscosity of concrete mixture, which leads to pulling the printer part when the aggregate moves. Finally, at the third trial it was decided to print 10 layers at a time, and keep the structure cured for some time till it gains certain level of robustness. The printing of the next layers started the next day (Figure 3a), and for the structure with 0.3 m in height it took altogether 3 days for printing, and plus one day of curing (Figure 3b).

a) Day 2   b) Day 4

Figure 3 – 3D printing process

Finally, the inner voids of the ready structure was reinforced and pured with heavy concrete (Figure 4). To make the rebar evenly installed in height of structure, it was hanged using metal wires.

Figure 4 – Reinforcing and pouring the voids with heavy concrete

4. Conclusions

In this study, we successfully printed a street flowerbed using a 3D printer and a custom-made concrete mixture. The workability test showed that the selected mixture meets the requirements for workability, and the compression test indicated that the concrete has a compressive strength of around 10 MPa, corresponding to the concrete grade of M100. The 3D printing process required several trials to find the optimal mode of printing for the chosen concrete composition, and it took 3 days to print the structure and one day for curing. The inner voids of the structure were reinforced with a knitted frame made of rebar and filled with heavy concrete.

The results of this study demonstrate the feasibility of using 3D printing technology for the production of concrete structures, which can be used for small repairs or as a permanent formwork. The technology allows for the creation of complex shapes and designs, which can be customized to meet specific requirements. However, further research is needed to optimize the printing parameters and to improve the strength and durability of the printed structures.

References

1. 3D printing of reinforced concrete elements: Technology and design approach / D. Asprone, F. Auricchio, C. Menna, V. Mercuri // Construction and Building Materials. — 2018. — Vol. 165. — P. 218–231. https://doi.org/10.1016/j.conbuildmat.2018.01.018
2. Environmental and economic assessment on 3D printed buildings with recycled concrete / Y. Han, Z. Yang, T. Ding, J. Xiao // Journal of Cleaner Production. — 2021. — Vol. 278. — P. 123884. https://doi.org/10.1016/j.jclepro.2020.123884
3. Prospects for the use of a 3D printer in construction / A.O. Torshin, E.N. Potapova // Advances in chemistry and chemical technology. — 2016. — Vol. XXX, No. 7. — P. 118–120.
4. A Study on the Importance and Application of 3D Printing Technology for Street Furniture Manufacturing / S.H. Lee, T.H. Lee, H.S. Lim // Journal of the Korea Academia-Industrial cooperation Society. — 2020. — Vol. 21, No. 4. — P. 509–517. https://doi.org/10.5762/KAIS.2020.21.4.509
5. Use of 3D printing in Furniture Production / M. Aydin // Conference: International Symposium on Innovative Technologies in Engineering and Science. — Isparta, Turkey: Süleyman Demirel University, 2015.
6. 3D Construction Printer «AMT» S-6045 M [Electronic resource] / AMT // Additive Manufacturing Technologies. — [2023]. — Mode of access: https://www.amt-print.com/3d-printers/s-6045m/ (accessed date: 02.06.2022).
7. GOST 23732-2011 Water for concrete and mortars. Specifications. — 2011.
8. GOST 31108-2016 Common cements. Specifications. — 2017.
9. GOST 8736-2014 Sand for construction works. Specifications. — 2015.
10. GOST 30459-2008 Admixtures for concretes and mortars. Determination and estimate of the efficiency. — 2011.
11. GOST 8267-93 Crushed stone and gravel of solid rocks for construction works. Specifications. — 2018.

12. GOST R 58767-2019 Mortars. Test methods using reference specimens. — 2019.
13. GOST 10180-2012 Concretes. Methods for strength determination using reference specimens. — 2012.
14. GOST 26633-2015. Heavy-weight and sand concretes. Specifications. — 2019.

Information about authors:

Gulnaz Zhairbaeva – Master of Technical Sciences, School of Architecture and Construction, D. Serikbayev East Kazakhstan Technical University, Ust-Kamenogorsk, Kazakhstan, gulnaz.w@mail.ru

Zulfiya Aubakirova – Master of Technical Sciences, School of Architecture and Construction, D. Serikbayev East Kazakhstan Technical University, Ust-Kamenogorsk, Kazakhstan, aubakirova.zulfiya@mail.ru

Yana Ivashina – Bachelor Student, D. Serikbayev East Kazakhstan Technical University Ust-Kamenogorsk, Kazakhstan, yana11062002@gmail.com

Alexandr Soldun – Bachelor Student, D. Serikbayev East Kazakhstan Technical University, Ust-Kamenogorsk, Kazakhstan, solduna@mail.ru

Alina Makienko – Bachelor Student, D. Serikbayev East Kazakhstan Technical University, Ust-Kamenogorsk, Kazakhstan, ali1234ali1234@mail.ru

Author Contributions:

Gulnaz Zhairbaeva – concept, methodology, funding acquisition.
Zulfiya Aubakirova – drafting, resources, interpretation.
Yana Ivashina – data collection, modeling.
Alexandr Soldun – visualization, editing.
Alina Makienko – testing, analysis

Dam Site Characterization Based on Land Use and Land Cover Changes in Urban Catchments. A Case of the Msimbazi Catchment in Dar es Salaam, Tanzania

Timoth Mkilima*

Department of Environmental Engineering and Management, University of Dodoma, P. O. Box 259, Dodoma, Tanzania
*Correspondence: tmkilima@gmail.com

Abstract. Site characterization is crucial for the location and design of dams because it offers data for risk assessments and the planning and implementation of remediation measures. This study looked into the potential use of GIS-based methods for the characterization of dam sites. Satellite pictures were used to verify the catchment delineation results. The catchment slope, the number of networks in the sub-basin, and the land surface cover were all taken into consideration while choosing a location for a dam. From the findings, five possible dam site locations — Kisarawe (upstream), Magomeni, Kinyerezi, Jangwani, and Pugu sub-catchments — were identified. The Kisarawe sub-basin upstream has the largest prospective location (covering an area of around 89.89 km^2) since it has a less populated and developed area, which would allow for enough room to construct a dam while protecting the downstream from frequent flooding. According to the capacity and other requirements of the receiving stream downstream, the chosen dam locations could hold approximately 75.15% of the runoff produced in the catchment before releasing it at a controlled rate. The outcomes of the study demonstrate further the effectiveness of geographic information systems in determining the characteristics of dam sites and in designing sustainable dams that take land surface cover into account.

Keywords: site characterization, geographical information system, dam sustainability, land use land cover, engineering design, urbanization.

1. Introduction

Dams are huge hydraulic structures that date back thousands of years and are still used today to provide water for irrigation, industry, and home use. Moreover, dams are well-known as a means of storing water for hydroelectric power generation and river traffic. The type of land surface cover, however, can have a big impact on dam sites. Changes in the land surface cover have a significant likelihood of impacting evapotranspiration rates and surface runoff, and they may also have an impact on infiltration and stream discharge. To be more precise, land cover influences how quickly a sand dam reaches its storage capacity as well as how quickly that storage is used up [1]. Therefore, if a dam location site has been poorly selected, it can have several negative effects, including the risk of erosion leading to mudslides and landslides, the potential for receiving either high or low flows that were not anticipated during the design process (potential failure), as well as be linked to significant negative economic benefits. Consequently, one of the most important steps in creating sustainable dams is to consider the spatial distribution of reservoirs while choosing the placement of the dam.

Development activities alter the land cover in urbanizing catchments, turning it mostly into impermeable surfaces like tarmac roads, pavements, rooftops, and so on. More stormwater runs on the surface and moves quickly toward a neighboring stream as a result of the increase in impervious surfaces than it would if it were to move underground [2-3]. This situation results in so-called flash floods because an enormous amount of stormwater runoff must be absorbed in a stream at once,

exceeding the stream's capacity [4]. The primary aim in many research involving surface waters, particularly streams, is flowing channel identification [5]. Depending on the developed flow routes, the direction of the flow and flow discharge can also be calculated. For many years, catchment flow routes have been automatically extracted using the digital elevation model (DEM) [6-7].

DEM is used as an input to extract stream networks and depicts the terrain's 3D geometry [8]. The DEM can be accessed with various resolutions on a number of open-source web forums. DEMs with higher resolution are preferred because they produce more accurate findings [9]. Sinks (depressions) are present in DEM, which signifies that certain locations lack data. To create a continuous drainage network, the sinks can be eliminated by interpolating the values of the neighboring pixels. By using the Fill Sinks tool during the catchment delineation, ArcGIS offers an automated method of filling the sinks [10–12]. In the realm of earth science, drainage networks, along with their channel connections and watersheds, are generally recognized as fundamental ideas. Prior to now, topographic maps and aerial photos were processed manually as part of the catchment delineation procedures. The usage of Geospatial Information Systems (GIS) has largely replaced human labor in the present thanks to technological innovation that makes it possible to employ sophisticated instruments [13-14].

Geography, civil engineering, computer science, land use planning, and environmental science are just a few of the academic and technological sectors that have been involved in the development of GIS into a mature study and application area throughout the years. When it comes to spatial queries that may be utilized to enhance location research, GIS is regarded as being extremely helpful. Moreover, GIS will play a crucial role in the creation and use of future location models [15]. Before deciding where to build a dam and planning it, it is crucial to carry out a site characterization that requires data collecting, field research, and interpretation. The majority of site characterization techniques, however, are both time- and money-consuming and relatively expensive. Therefore one of the interesting ways for the characterization of dam sites can be a combination of various GIS technologies.

This study explores the possible use of a variety of GIS-based techniques for the characterization of dam sites. The Msimbazi watershed in Dar es Salaam, Tanzania, is delineated using GIS-based methodologies for catchment delineation in order to find prospective locations for flood mitigation dams. The US Army Corps of Engineers Geospatial Hydrologic Modeling Extension (HEC-GeoHMS) plugin for ArcGIS was utilized for the study to drain streams in the study basin. Using satellite imagery, the conclusions of the catchment delineation were verified. The Landsat photos were used for the geographic study of the surface land use and land cover. The catchment slope, the number of networks in the sub-basin, and the land surface cover were taken into consideration when choosing a location for a dam.

2. Materials and methods

2.1 Study area description

The Mzimbazi catchment is situated in Dar es Salaam, Tanzania, and is one of the largest in the region. It is located between latitudes 6°27' and 7°15 South of the Equator and between longitudes 39° and 39°33' East of Greenwich. The Msimbazi river flows over the city of Dar es Salaam, originating from the higher portions of the Kisarawe district in the Coastal region, before emptying into the Indian Ocean. As an ungauged catchment, Mzimbazi is frequently affected by floods during the wet season, causing significant damage to low-lying areas. The catchment is subject to land-use changes due to construction activities such as settlements. The basin experiences a tropical climate, with two rainy seasons from November to January and March to May, and an average annual precipitation of 1,150 mm. Daily temperatures range from 17 to 33 ^{0}C.
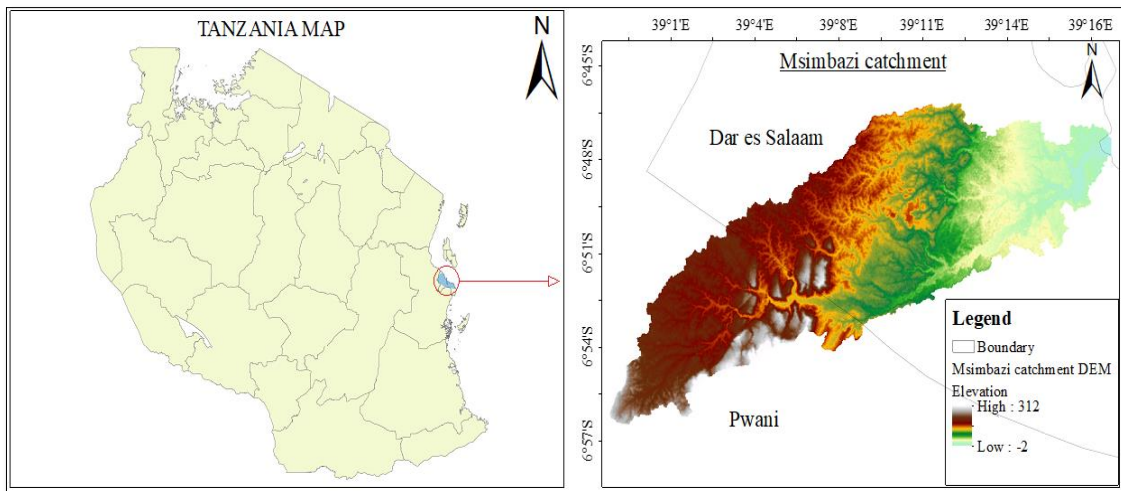
Figure 1 – Study area

2.2 Datasets

To define the catchment, the HEC-GeoHMS plugin for ArcGIS 10.5 was used. After that, the LP DAAC-controlled online open-source database was used to obtain the ASTER GDEM with 30m resolution DEM (NASA Land Processes Distributed Active Archive Center). The watershed's streams and bounds were assessed using Google Earth-based inquiry methodologies while using the stream shapefile of the catchment that was obtained from Google maps for DEM-Reconditioning. The Google Earth Pro desktop version 7.3.2.5776 provided the images with a resolution of 4800 x 2718 (64-bit). For the analysis of land use and land cover, Landsat photos were downloaded from the United States Geological Survey (USGS) website. The estimation of discharge for each sub-catchment and the entire catchment was done using the rational method. The Tanzania Meteorological Agency's (TMA) recording of the 100-year extreme rainfall event that occurred on December 20, 2011, served as an input for estimating runoff flow.

2.3 DEM preprocessing

By extracting the geomorphologic properties of the catchment, ArcGIS 10.5 was used to generate catchment layouts and produce natural flow patterns (drainage routes). The output was then overlaid against a few chosen georeferenced shapefiles in ArcGIS, and the findings were verified. The full process is summarized in Figure 2 below [16].
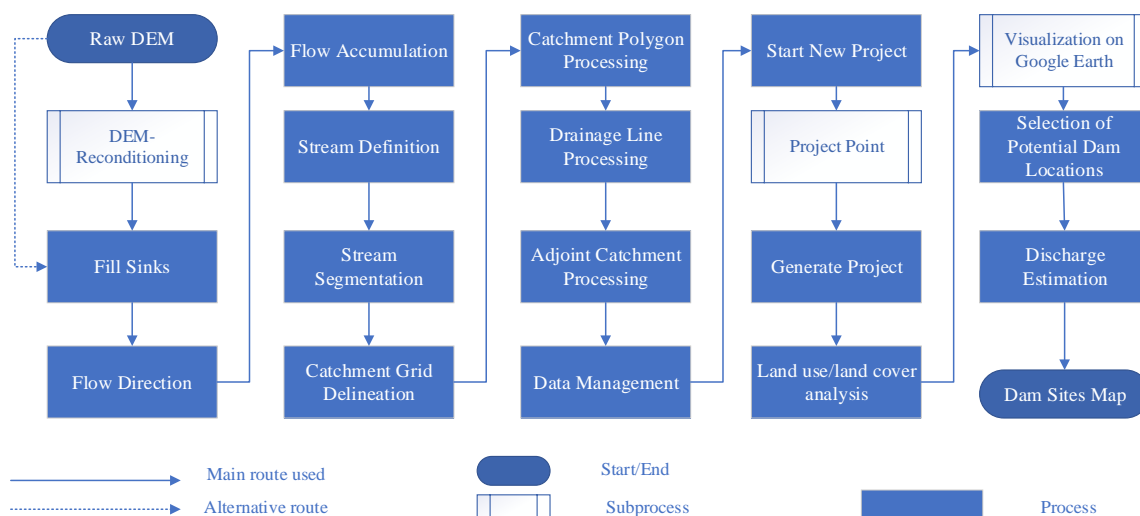

Figure 2 – General study flowchart

The DEM-Reconditioning was the initial stage of the catchment delineation. The area downstream of the Msimbazi catchment is relatively flat, and there are numerous structures (such as bridges) that cross the streams (Figure 3). As a result, the process of developing flow paths may run into difficulties when it reaches these areas [17] and those where the streams are covered by structures because it may be unable to determine the precise path to take. As a result, this study fixed the delineated streams into their precise routes using the DEM-Reconditioning technique and the catchment's accessible streams shape-file. Afterward, sinks in the DEM were filled using the Fill Sinks tool in HEC-GeoHMS tools. This was done to make sure that if cells with higher elevations are located close to cells with lower elevations, the flow of water will be impeded and trapped in the lower-height cells, making it impossible for the water to exit the cells.

The further processes included catchment grid delineation, catchment polygon processing, drainage line processing, adjoint catchment processing, flow direction, flow accumulation, stream definition (where the stream threshold is set), stream segmentation, and stream segmentation. The direction of the sharpest slope, or largest drop, from each cell, determines the flow direction. It is calculated using the formula in Eq (1).

$$\text{Maximum\_drop} = \frac{\text{change\_in\_z-value}}{\text{distance} * 100} \tag{1}$$

2.4 Project development

The design of HEC-GeoHMS incorporates more sophisticated features for the creation of catchment boundaries and streams. Following the DEM preprocessing, the projects for the entire catchment and each of the different sub-basins were created using the Project Setup submenu. A project was started using the Start New Project tool, data was set using the Data Management tool, and a project was generated using the Create Project tool. Runoff and water quality simulation require precise identification of the watershed. However, due to significant depressions and minute elevation changes in local-scale plains (Figure 3), the accuracy of digital elevation models (DEMs) continues to be problematic and may not produce accurate drainage networks [18].

Figure 3 – Real scenarios of catchment delineation challenges

2.5 Land use/ land cover analysis

The examination of land use and land cover helped choose the runoff coefficient. The high-resolution Google Earth photos and the Interactive Supervised Classification technique in ArcGIS were used to assess the land surface cover, which is defined from the existing use of the land, with the aid of having adequate information on the study catchment. The analysis was limited to the primary five land use/land cover classifications (Table 1), and the impervious coefficients were allocated in accordance with the guidelines provided by the National Land Cover Database 2011 Legend [19]. The watershed delineation data and the land use/land cover results were then integrated in order to assess the selected dam sites in terms of the state of land surface cover.

Table 1 – Definition of the land use/land cover classes

Category	Description
Water	Areas of open water that are frequently covered by less than 25% of soil or vegetation.
Low-intensity development	A variety of places are made up of vegetation, built objects, grassland, arable land, and cultivated crops. Surfaces that are impervious make up 20% to 49% of the overall cover.
Medium-intensity development	greenery mixed with artificial materials. Impervious surfaces account for 50% to 79% of the overall cover.
High-intensity development	Areas that have been extensively developed and are home to a significant population. 80% to 100% of the surface is made up of impervious surfaces.
Forest	Generally, more than five meters tall trees dominate areas.

2.6 Dam site selection

Sites for dams were selected based on the catchment slope, land surface cover (as confirmed by satellite photos), and the number of networks in the sub-basin. Also, consideration was given to where to construct dams so that they wouldn't directly obstruct the catchment's primary stream of water flow. The general strategy is designed to keep the mainstream flowing normally throughout the flooding season while the dams either hold back or keep the excess runoff. This strategy is advantageous because it gives the mainstream enough time to manage the remaining runoff volume because enough runoff is captured in the dams during the flooding (high flow) season.

3. Results

As was already mentioned, one of the most important aspects of the study was the catchment delineation procedure, which was made possible in large part by the use of the HEC-GeoHMS software as a plugin for the ArcGIS 10.5 program (Figure 4). Some of the geomorphological datasets that were gathered during the process include the delineation of stream networks, the main catchment boundaries, the demarcation of sub-catchment boundaries, slope profiles, and stream cross-sections. It is also important to note that the HEC-GeoHMS produced sub-basins and streams that were well-drained and easily discernible when choosing the probable dam site locations.

Following the DEM processing, 151 tiny sub-basins with 151 streams were generated. According to the hydro-filled DEM, the elevation of the research catchment ranges from 0 to 312 meters, indicating that it is situated in a low-lying area. The lowest elevation is situated downstream of the watershed when its departure pours water into the Indian Ocean. Additionally, the slope changes gradually throughout the basin. The presence of man-made structures like bridges and flat areas makes it harder to determine flow direction precisely since they change the natural trend of elevation.

The Msimbazi basin's land use/land cover classes were successfully classified using the Interactive Supervised Classification on a few selected Landsat images. The Msimbazi catchment was divided into five land use/land cover categories: water, developed medium intensity, developed low intensity, and vegetation. The land use/land cover analysis revealed that the intensity of development increased downstream and decreased upstream (in the Kisarawe hills), where the watershed starts. The developed, low-intensity scenario predominated upstream of the basin, whereas the developed, high-intensity scenario was more easily apparent downstream.
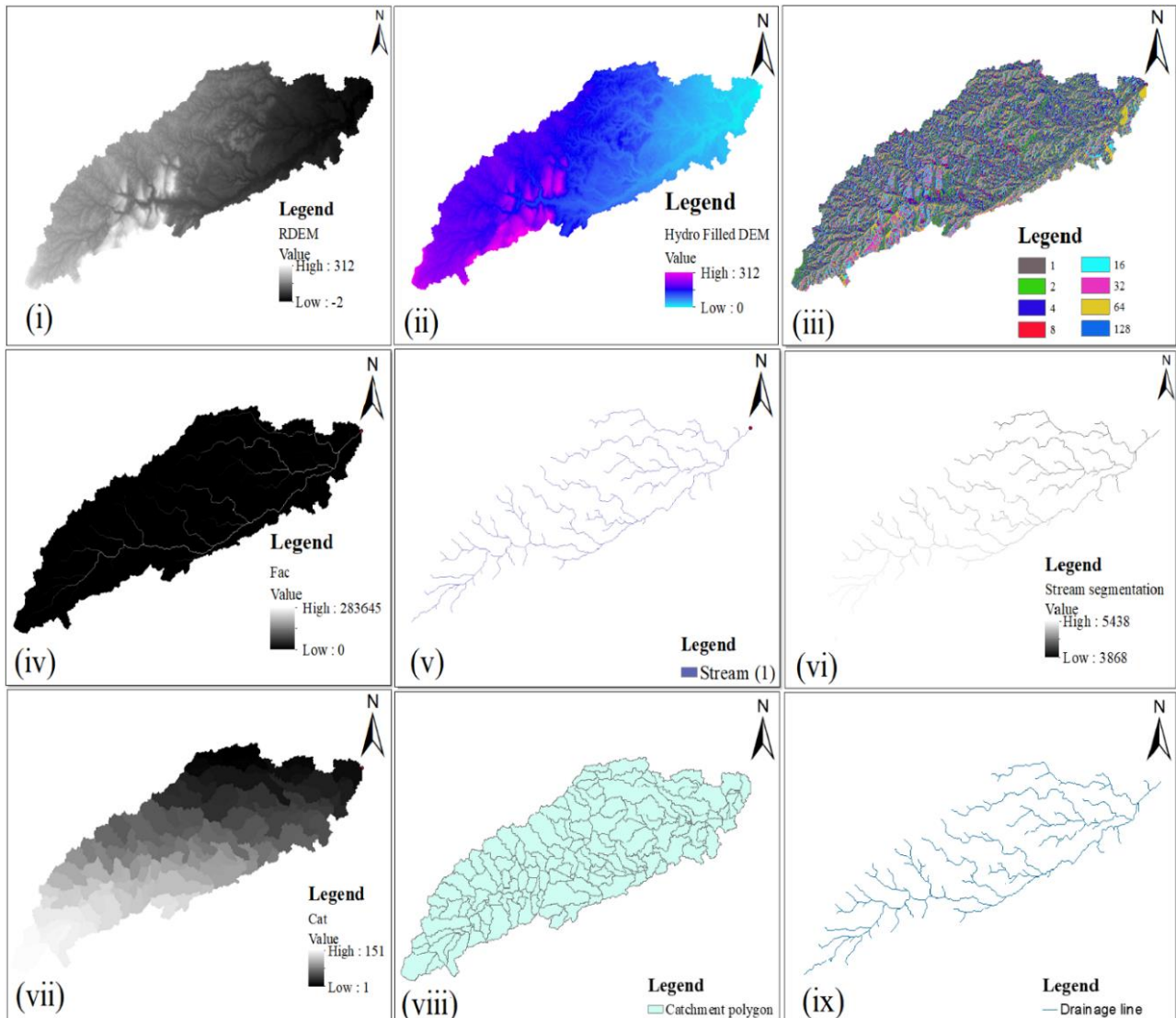

Figure 4 – Steps involved in the catchment delineation (i) input DEM (ii) filling process (iii) flow direction (iv) flow accumulation (v) stream definition (vi) stream segmentation (vii) catchment grid delineation (viii) catchment polygon processing (ix) drainage line processing

After an investigation using a combination of catchment delineation, land use/land cover analysis, and high-resolution Google Earth images, five potential dam site locations were retrieved, including the Kisarawe sub-basin, the Magomeni sub-basin, the Kinyerezi sub-basin, the Jangwani sub-basin, and the Pugu sub-basin (Figures 5, Figure 6 and 7). The streams that contain a substantial number of substreams before emptying into the main channel are where the dam sites' exits are typically found. The site with the highest promise is upstream in the 89.89 km^2 Kisarawe sub-basin; it is less populous and less developed than other potential sites, allowing for the construction of a dam and safeguarding the downstream from recurrent flooding.
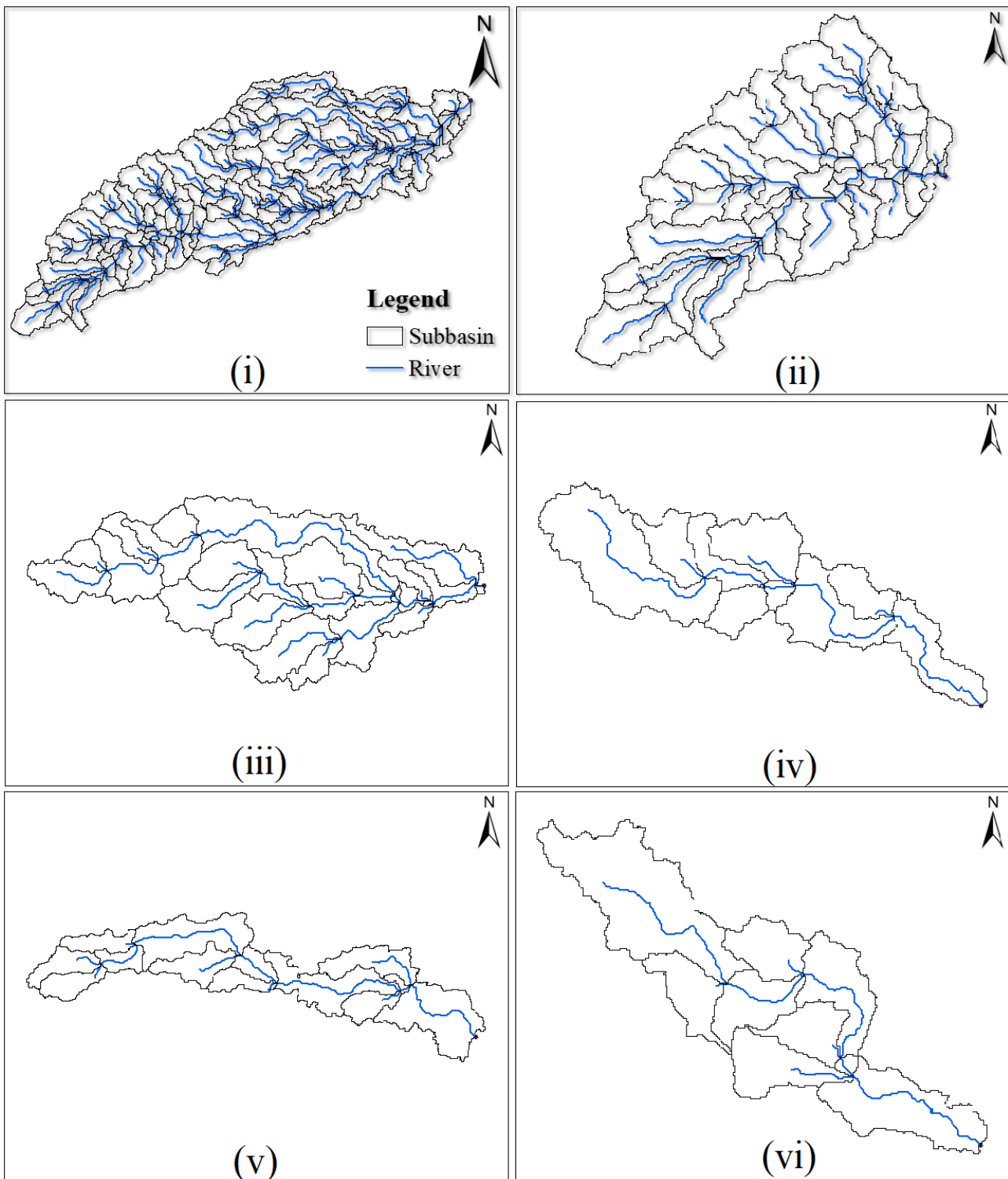
Figure 5 – Delineated subbasins for the selected dam sites (i) number 5 (ii) number 7 (iii) number 9 (iv) number 11 (v) number 13

A summary of the classified land use/land surface cover for each sub-catchment, together with the delimited sub-catchments, is shown in Figure 6. Each sub-catchment has been given the appropriate land surface cover characteristics, as seen in Figure 6. The design team can benefit greatly from knowing the current status of the land surface cover in a catchment before installing a dam in order to foresee potential problems caused by changes in the land surface cover that could influence the operability of the dam. It is crucial to stress that changes in land cover continue to have an impact on weather and climate on a local to a global scale by changing how energy, and water move between the land and the atmosphere.
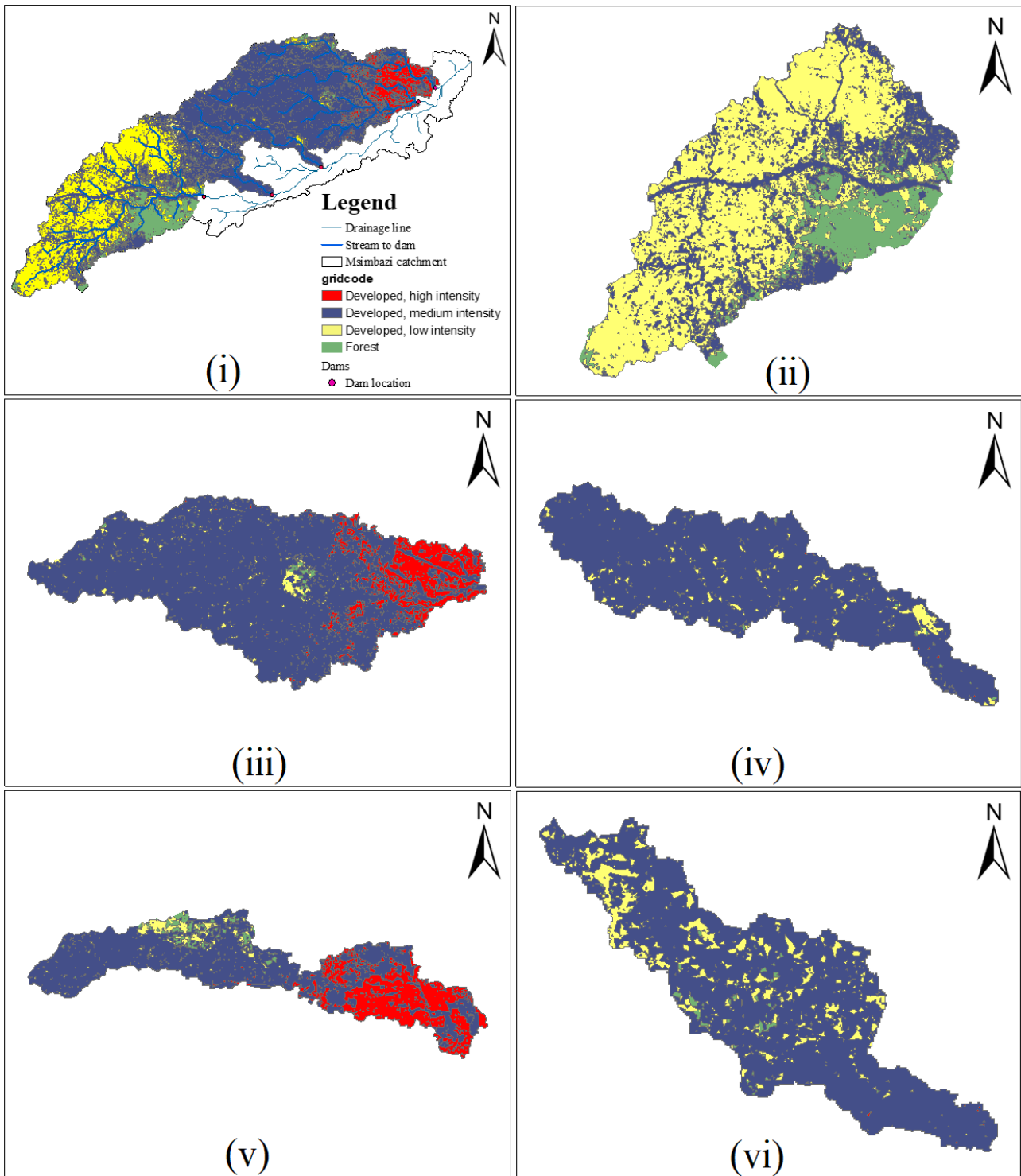
Figure 6 – Distribution of land use and land cover for each subbasin of the chosen sites (i) entire catchment (ii) Kisarawe sub-basin (iii) Magomeni subbasin (iv) Kinyerezi subbasin (v) Jangwani sub-basin (vi) Pugu sub-basin

Figure 7 summarizes the position of the chosen possible dam site as determined by HEC-Geo HMS. Additionally, clearly defined streams that contribute to each chosen dam site can be seen. It should be emphasized that rivers are the result of water moving through gravity from one elevation to another. When rain falls on land, it either soaks into the soil or turns into a runoff, which travels to the sea by flowing downhill into rivers and lakes. The land is not completely flat in most landscapes; it slopes in one or more directions. Small creeks are how flowing water initially makes its way downhill. Small creeks join to become larger streams and rivers as they move downward.

Figure 7 – Dam site locations: Streams only (left), streams with coverage (right)

4. Discussion

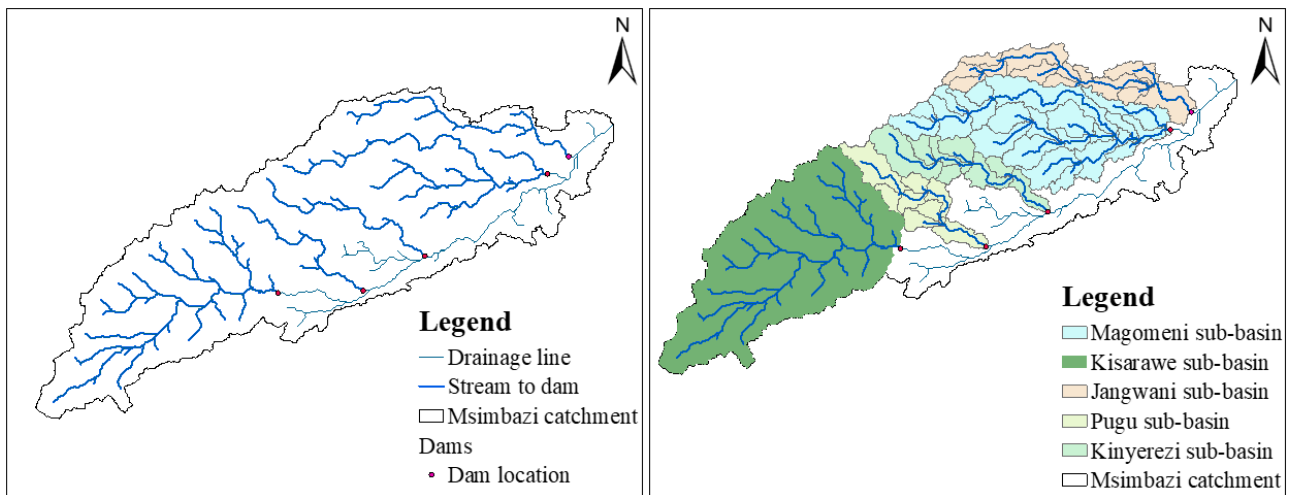The study's conclusions suggest a promising strategy for locating suitable dam locations inside catchments: combining DEM and HEC-GeoHMS methodologies. Remote Sensing (RS) and Geographical Information Systems (GIS) are frequently very useful in providing geospatial data for the evaluation of potential dam sites [20–23]. Additionally, having prior knowledge of the subject matter and technical competence are essential since they allow for the connection between theories and the actual situation on the ground, making it easy to identify potential dam sites [24–26]. 151 small sub-basins with 151 streams were produced after the DEM processing. According to the hydro-filled DEM, the elevation of the research catchment ranges from 0 to 312 meters, indicating that it is situated in a low-lying area. According to López-Dóriga and Jiménez [27], due to their low height, subsidence, and present low sediment supply on the one hand, and their high ecological and socioeconomic values on the other, low-lying coastal areas are high-risk sites for sea-level rise. The lowest elevation is situated downstream of the watershed when its departure pours water into the Indian Ocean. Moreover, the slope changes gradually throughout the basin. The presence of man-made structures like bridges and flat areas makes it harder to determine flow direction precisely since they change the natural trend of elevation.

The Msimbazi basin's land use/land cover classes were successfully classified using the Interactive Supervised Classification on a few selected Landsat images. The Msimbazi catchment was divided into five land use/land cover categories: water developed medium intensity, developed low intensity, and vegetation. The land use/land cover analysis revealed that the intensity of development increased downstream and decreased upstream (in the Kisarawe hills), where the watershed starts. The developed, low-intensity scenario predominated upstream of the basin, whereas the developed, high-intensity scenario was more easily apparent downstream. It should be emphasized that changes in the use of land and its cover have an impact on soil erosion, sediment loads, processes of land degradation, and microclimatic resources at the local level. Each of them directly affects how local societies make a living [28].

A combination of catchment delineation, land use/land cover analysis, and high-resolution Google Earth images was used in the investigation to identify five potential dam site locations, including the Kisarawe sub-basin, the Magomeni sub-basin, the Kinyerezi sub-basin, the Jangwani sub-basin, and the Pugu sub-basin. The streams where the dam sites' exits are located are often those with a sizable number of substreams before they empty into the main channel. The most promising option is the upstream Kisarawe sub-basin, which has a size of around 89.89 km^2 and is less populous and less developed than other probable sites. This makes it possible to build a dam there and shield the downstream from regular flooding. It is important to keep in mind that dams are constructed to safely contain huge volumes of water, which are then released for a number of uses, such as

agriculture, hydropower, recreation, water supply, flood control, inland navigation, and so forth. The choice of a dam location is necessary for a variety of operations including irrigation, hydropower, recreation, and water supply. Dam locations should be carefully chosen to increase project safety, shorten construction duration, and cut construction costs. As a result, choosing and assessing a variety of viable dam locations early in the construction phase is essential [29].

Considering the studies conducted in some other parts of the world [12-30-31], The geomorphological properties of a catchment can be easily extracted using GIS-based approaches. This study's objective was to include HEC-GeoHMS tools into the assessment process in order to further investigate how beneficial geo-based techniques are for assessing potential dam sites that are situated in catchments that have experienced flooding. During the installation process, the HEC-GeoHMS was sophisticated enough to detect the absence of Arc Hydro tools and then give the user the option of automatically installing Arc Hydro tools compatible with the version of ArcGIS already installed in the working system. Additionally, the Project Setup section of HEC-GeoHMS produced more hopeful results for catchment delineation following the DEM preprocessing, including streams that were more properly delineated. This approach provides a quick and efficient means to extract, map, and understand the catchment features for the goal of selecting suitable dam site locations, making it seem more practical than having to manually locate the necessary Arc Hydro tools. As was already mentioned, choosing the right dam sites is important for assuring project safety, cutting down on building time, and minimizing construction expenses. As a result, choosing and assessing a variety of viable dam locations early in the construction phase is crucial. Moreover, the ability to develop, modify, and manage pertinent thematic layers makes remote sensing and GIS valuable in choosing the location of dams and reservoirs.

5. Conclusions

The potential applicability of geographical information system-based approaches for dam site characterization has been investigated for a case of the Msimbazi catchment in Dar es Salaam, Tanzania. From the results, total area coverage of 267.24 km^2 was delineated. The following can be concluded from the results:

− An essential component of the study was the processing of Landsat and Google Earth images to describe the land surface attributes of the study catchment for runoff-affecting elements as well as identify any potential practical difficulties for precise catchment demarcation.

− Five land use classes – water, high-intensity development areas, medium-intensity development regions, low-intensity development areas, and vegetation cover—were identified in the analysis using the supervised technique.

− Development activity is more intense downstream of the river and less so upstream. The genuine state of the catchment is revealed by this phenomenon.

− According to the capacity and other requirements of the receiving stream downstream, the chosen dam locations could hold approximately 75.15% of the runoff produced in the catchment before releasing it at a controlled rate.

− Dams can be an important engineering tool in the fight against flooding, especially if they are strategically placed and well-made. In addition, dams built in metropolitan areas can be used for recreational activities, the generation of small amounts of energy, the prevention of soil erosion, and the extension of river flow while preserving the ecosystem of sporadic flashy rivers.

References

1. Assessing the Impact of Land Cover, Soil, and Climate on the Storage Potential of Dryland Sand Dams / J.A. Eisma, S. Saksena, V. Merwade // Frontiers in Water. — 2021. — Vol. 3. — P. 671455. https://doi.org/10.3389/frwa.2021.671455
2. Optimization of Impervious Surface Space Layout for Prevention of Urban Rainstorm Waterlogging: A Case Study of Guangzhou, China / Yu, Zhao, Fu // International Journal of Environmental Research and Public Health. — 2019. — Vol. 16, No. 19. — P. 3613. https://doi.org/10.3390/ijerph16193613

3. Characteristics of impervious surface and its effect on direct runoff: a case study in a rapidly urbanized area / C. Li, M. Liu, Y. Hu, M. Zong, M. Zhao, M. Todd Walter // Water Supply. — 2019. — Vol. 19, No. 7. — P. 1885–1891. https://doi.org/10.2166/ws.2019.064

4. Flood and Flash Flood Geo-Hazards in Malaysia / F.S. Buslima, R.C. Omar, T.A. Jamaluddin, H. Taha // International Journal of Engineering & Technology. — 2018. — Vol. 7, No. 4.35. — P. 760–764.

5. Efficient identification of preferential flow path in heterogeneous media based on stream function / T. Nan, L. Xue, J. Wu // Journal of Hydrology. — 2019. — Vol. 577. — P. 123961. https://doi.org/10.1016/j.jhydrol.2019.123961

6. Evaluating preprocessing methods of digital elevation models for hydrological modelling / W. Lidberg, M. Nilsson, T. Lundmark, A.M. Ågren // Hydrological Processes. — 2017. — Vol. 31, No. 26. — P. 4660–4668. https://doi.org/10.1002/hyp.11385

7. Digital Elevation Model Quality Assessment Methods: A Critical Review / L. Polidori, M. El Hage // Remote Sensing. — 2020. — Vol. 12, No. 21. — P. 3522. https://doi.org/10.3390/rs12213522

8. Evaluating the Effects of Digital Elevation Models in Landslide Susceptibility Mapping in Rangamati District, Bangladesh / Y.W. Rabby, A. Ishtiaque, Md.S. Rahman // Remote Sensing. — 2020. — Vol. 12, No. 17. — P. 2718. https://doi.org/10.3390/rs12172718

9. Very high-resolution digital elevation models: are multi-scale derived variables ecologically relevant? / K. Leempoel, C. Parisod, C. Geiser, L. Daprà, P. Vittoz, S. Joost // Methods in Ecology and Evolution. — 2015. — Vol. 6, No. 12. — P. 1373–1383. https://doi.org/10.1111/2041-210X.12427

10. Automatic ArcHydro for Watershed delineation / C. Kraemer, S.S. Panda // Proceedings of the 2009 Georgia Water Resources Conference. — Oakwood, Georgia: University of Georgia, 2009. — P. 6.

11. Automatic Delineation of Drainage Networks and Catchments using DEM data and GIS Capabilities: a case study / F. Akram, M.G. Rasul, M.M.K. Khan, M.S.I.I. Amir // Proceedings of the 18 th Australasian Fluid Mechanics Conference. — Launceston, Australia: Australasian Fluid Mechanics Society, 2012. — P. 344–347.

12. Catchment Area Delineation Using GIS technique for Bekhma Dam / M.N. Abdulla // Proceedings of the TS09C - Spatial Information Processing II. — Marrakech, Morocco: 2011. — P. 5335.

13. Mapping outlet points used for watershed delineation onto DEM-derived stream networks: MAPPING POINTS ONTO DEM-DERIVED STREAM NETWORKS / J.B. Lindsay, J.J. Rothwell, H. Davies // Water Resources Research. — 2008. — Vol. 44, No. 8. https://doi.org/10.1029/2007WR006507

14. Automated Watershed Evaluation of Flat Terrain / S.W. Al-Muqdadi, B.J. Merkel // Journal of Water Resource and Protection. — 2011. — Vol. 03, No. 12. — P. 892–903. https://doi.org/10.4236/jwarp.2011.312099

15. Geographical information systems and location science / R.L. Church // Computers & Operations Research. — 2002. — Vol. 29, No. 6. — P. 541–562. https://doi.org/10.1016/S0305-0548(99)00104-5

16. Aspects of embankment dams stability considering the impact of land use changes and climatic conditions in catchments / T. Mkilima. — Astana, Kazakhstan: L.N. Gumilyov Eurasian National University, 2022. — 302 p.

17. Environmental Applications of Digital Terrain Modeling / J.P. Wilson. — Chichester, UK: John Wiley & Sons, Ltd, 2018. — 360 p. https://doi.org/10.1002/9781118938188

18. A Method of Watershed Delineation for Flat Terrain Using Sentinel-2A Imagery and DEM: A Case Study of the Taihu Basin / L. Li, J. Yang, J. Wu // ISPRS International Journal of Geo-Information. — 2019. — Vol. 8, No. 12. — P. 528. https://doi.org/10.3390/ijgi8120528

19. The National Land Cover Database / C.H. Homer, J.A. Fry, C.A. Barnes // U.S. Geological Survey Fact Sheet 2012-3020. — Virginia, USA: 2012. — P. 4.

20. GIS and remote sensing techniques in Controlled Environment Agriculture: A review / A. M. Al-Ismaili // Journal of Agricultural and Marine Sciences [JAMS]. — 2021. — Vol. 26, No. 2. — P. 10–23. https://doi.org/10.53541/jams.vol26iss2pp10-23

21. Environmental Modelling with GIS and Remote Sensing / A. Skidmore. — Florida, USA: CRC Press, 2002. — 286 p.

22. Remote Sensing and GIS Integration / E. Nizeyimana // Managing Human and Social Systems. — Florida, USA: CRC Press, 2020. — P. 5.

23. Groundwater potential assessment using GIS and remote sensing: A case study of Guna tana landscape, upper blue Nile Basin, Ethiopia / T.G. Andualem, G.G. Demeke // Journal of Hydrology: Regional Studies. — 2019. — Vol. 24. — P. 100610. https://doi.org/10.1016/j.ejrh.2019.100610

24. A GIS-based approach for identifying potential sites for harvesting rainwater in the Western Desert of Iraq / A. Adham, K.N. Sayl, R. Abed, M.A. Abdeladhim, J.G. Wesseling, M. Riksen, L. Fleskens, U. Karim, C.J. Ritsema // International Soil and Water Conservation Research. — 2018. — Vol. 6, No. 4. — P. 297–304. https://doi.org/10.1016/j.iswcr.2018.07.003

25. GIS-Based Site Selection for Check Dams in Watersheds: Considering Geomorphometric and Topo-Hydrological Factors / O. Rahmati, Z. Kalantari, M. Samadi, E. Uuemaai, D.D. Moghaddam, O.A. Nalivan, G. Destouni, D. Tien Bui // Sustainability. — 2019. — Vol. 11, No. 20. — P. 5639. https://doi.org/10.3390/su11205639

26. Identification of Potential Sites for a Multi-Purpose Dam Using a Dam Suitability Stream Model / Z. Shao, Z. Jahangir, Q. Muhammad Yasir, Atta-ur-Rahman, S. Mahmood // Water. — 2020. — Vol. 12, No. 11. — P. 3249. https://doi.org/10.3390/w12113249

27. Impact of Relative Sea-Level Rise on Low-Lying Coastal Areas of Catalonia, NW Mediterranean, Spain / U. López-Dóriga, J.A. Jiménez // Water. — 2020. — Vol. 12, No. 11. — P. 3252. https://doi.org/10.3390/w12113252
28. The Impact of Land Use and Land Cover Changes on the Nkula Dam in the Middle Shire River Catchment, Malawi / M. Kapute Mzuza, W. Zhang, F. Kapute, X. Wei // Earth Observation and Geospatial Analyses [Working Title]. — London, UK: IntechOpen, 2019. https://doi.org/10.5772/intechopen.86452
29. Suitable dam site identification using GIS-based MCDA: a case study of Chemoga watershed, Ethiopia / Y.G. Hagos, T.G. Andualem, M.A. Mengie, W.T. Ayele, D.A. Malede // Applied Water Science. — 2022. — Vol. 12, No. 4. — P. 69. https://doi.org/10.1007/s13201-022-01592-9
30. How large is the Upper Indus Basin? The pitfalls of auto-delineation using DEMs / A. Khan, K.S. Richards, G.T. Parker, A. McRobie, B. Mukhopadhyay // Journal of Hydrology. — 2014. — Vol. 509. — P. 442–453. https://doi.org/10.1016/j.jhydrol.2013.11.028
31. Delineation of groundwater potential zones in Theni district, Tamil Nadu, using remote sensing, GIS and MIF techniques / N.S. Magesh, N. Chandrasekar, J.P. Soundranayagam // Geoscience Frontiers. — 2012. — Vol. 3, No. 2. — P. 189–196. https://doi.org/10.1016/j.gsf.2011.10.007

Information about the author:
Timoth Mkilima – PhD, Lecturer, Department of Environmental Engineering and Management, University of Dodoma, P. O. Box 259, Dodoma, Tanzania, tmkilima@gmail.com

Author Contributions:
Timoth Mkilima – concept, methodology, resources, data collection, testing, modeling, analysis, visualization, interpretation, drafting, editing, funding acquisition.

Article

Experimental study on physical-mechanical characteristics of steel fiber reinforced concrete with worn rope fibers

Dias Kazhimkanuly[1,*], Valeriy Chernavin[2]

[1]Department of Civil Engineering, L.N. Gumilyov Eurasian University, Astana, Kazakhstan
[2]School of Architecture and Construction, D. Serikbayev East Kazakhstan Technical University, Ust-Kamenogorsk, Kazakhstan
*Correspondence: dias27049795@gmail.com

Abstract. This study examined the physical-mechanical properties of steel fiber reinforced concrete with different fiber orientations and vibration times. The concrete mixtures contained crushed stone, sand, Portland cement, Rheobuild 181A plasticizer, and 5 cm steel fibers with 2% reinforcement. Using steel fibers from worn ropes from Innotech LLP (Almaty, Kazakhstan) increased the average strength of concrete and improved its ductility, allowing for plastic failure instead of brittle failure. Joint mixing of steel fiber-reinforced concrete with randomly oriented fibers made from used cables increased the mean value of flexural strength. The concrete mixtures with a vibration time of 9 seconds showed the highest flexural strength, which was 2.1 times higher than that of concrete samples without fiber. These findings demonstrate the potential of steel fiber reinforcement to improve the mechanical properties of concrete, especially in applications requiring flexural strength.
Keywords: steel fiber, concretes, flexural strength, worn rope, joint mixing.

1. Introduction

Steel fiber reinforced concrete (SFRC) is a type of reinforced concrete that incorporates steel fibers into a specially designed concrete matrix [1], reducing the need for traditional reinforcement and providing technical and economic benefits in various construction applications [2]. The traditional SFRC production process involves preparing a concrete mix in a mixer, adding a specified amount of dispersed steel reinforcement, and mixing both components until the reinforcement is evenly distributed throughout the mixture. The SFRC mixture is then placed in forms or molds and subjected to vibration compaction. The components of traditional SFRC vary in composition, with a cement-to-sand ratio of 1:1.9 to 2.0, a water-to-cement ratio of 0.4 to 0.5, and the addition of plasticizing agents in amounts of 0.6 to 1.0% of the cement's weight. The parameters of the steel fiber reinforcement of the concrete mixture are characterized by values such as a fiber volume content of 2%, a geometric factor (ratio of fiber length to diameter) of 30 to 45, and a fiber diameter of 1.6 mm. Steel fiber-reinforced concrete (SFRC) has drawbacks like fiber clumping during mixing, limiting fiber length and reducing mixture homogeneity. The strength of SFRC is proportional to inter-fiber spacing which can be increased from 6-10 mm to 3-5 mm resulting in material strengthening up to 2.5 times. Traditional SFRC structures fail due to insufficient fiber anchoring with fibers over 80-100 geometric factor. Increasing fiber volume content by more than 3% causes fiber clumping, complicating compaction and reducing material strength [3]. Research is underway to solve these issues.

This study aims to investigate the influence of the manufacturing process of steel fiber-reinforced concrete (SFRC) using wire fiber obtained from discarded ropes on the strength of the

structure under bending. The main objective is to determine the optimal manufacturing process that maximizes the material's strength characteristics. To achieve this goal, bending tests were conducted, during which the strength parameters of the SFRC structure were measured. Discarded ropes were used as a source of wire fiber, which improved the material's characteristics. The research results may help optimize the SFRC production process and create stronger and more durable structures for use in construction.

The research tasks include:

− Investigating the strength of SFRC manufactured using the combined mixing method under bending.

− Conducting comparative analyses on the influence of fiber technological parameters on the main physical and mechanical characteristics of SFRC structures.

− Analyzing the results and comparing them with the findings of previous studies.

2. Methods

The concrete samples used in the study were composed of a combination of various components. The primary components used in the samples included 5-10 mm crushed stone, sand with a fineness modulus of 2.5, Portland cement with an activity of grade M450, Rheobuild 181A plasticizer, as well as tap water. Additionally, for the experiments, we used a fiber made from recycled cables from Innotech, LLP (Almaty, Kazakhstan) [4] to manufacture the SFRC samples. The fiber reinforcement percentage was 2%, with a fiber length of 5 cm.

The experimental program included [5-6]:

− Bending test of concrete samples under bending;

− The flexural strength estimation;

− Comparative analysis of the influence of fiber technological parameters.

Tests were conducted to determine the effect of vibration time of the samples, as well as its technical characteristics, on the flexural strength of SFRC.

To perform the bending test, reference samples were manufactured in the form of square prisms with dimensions of 100×100×400 mm according to [5]. Each series included three samples, with different vibration times: 3 and 9 seconds. The series manufacturing modes are depicted in Table 1 below.

Table 1 – Manufacturing modes

No. of series	Method	Fiber length, см	Features of samples manufacturing
1	Volumetric-arbitrary orientation	5	With optimal compaction time on the vibrating table
2	Volumetric-arbitrary orientation	5	With a compaction time on the vibrating table 3 times longer than optimal

To accelerate the strength gain of concrete samples, we employed a technique known as thermal-moisture treatment. This method involved utilizing a steam curing chamber, specifically the KUP-1 (as depicted in Figure 1), and following a specific treatment cycle. The cycle consisted of a holding period of 2-3 hours, with a gradual temperature increase at a rate of 25-30 °C per hour. This was followed by isothermal heating at 80-90 °C for 6-8 hours, and then a temperature decrease at a rate of 30-40 °C per hour. After this meticulous process, the concrete achieved a strength level ranging from 70-100% of its ultimate strength at 28 days. Prior to testing, a thorough visual inspection was conducted to identify any potential defects in the concrete samples. Additionally, linear measurements were taken using a caliper with a high level of accuracy, with an error margin of no more than 1%. This ensured precise and reliable results for evaluating the strength gain of the concrete samples after the thermal-moisture treatment.

Figure 1 – Universal steaming chamber KUP-1

Samples, at a vibration time of 3 and 9 seconds, made to determine the flexural strength are shown in Figure 2.

Figure 2 – SFRC samples with vibration times of 3 (left) and 9 (right) seconds

The measurement results were recorded in the testing journal. A hydraulic press (2PG-10) was used to determine the flexural strength. Each sample was placed on two supports and loaded until it fractured at a constant rate of stress increase (0.05 ± 0.01) MPa per second, with the load applied at the mid-span and evenly distributed over the sample width. The setup configuration is illustrated in Figure 3.
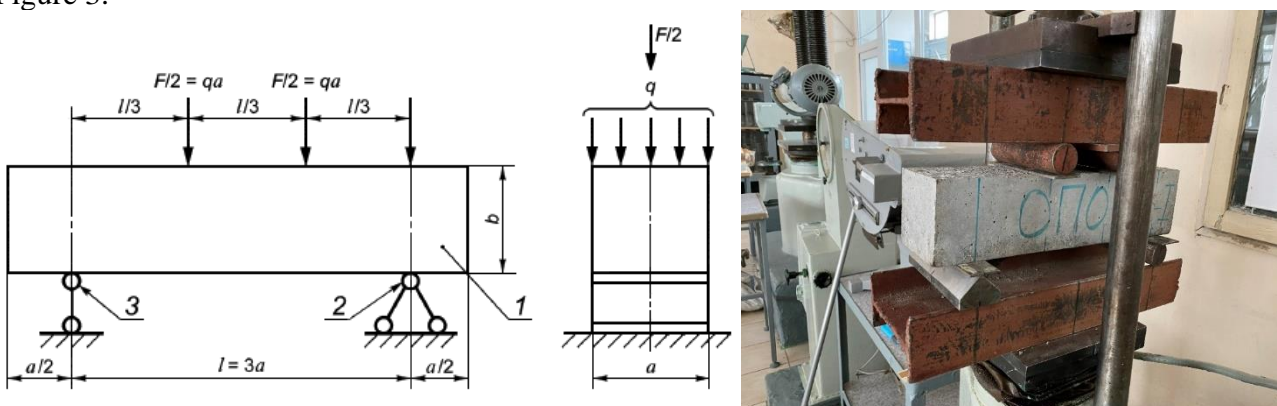

Figure 3 – Test setup: 1 – sample; 2 – hinged and fixed bearing; 3 – pivot bearing; a – width and height of sample; F – load; q – evenly distributed load; l – distance between supports.

The flexural strength (R_{tb}, MPa) was determined according to the following equation [5]:

$$R_{tb} = \delta \frac{Fl}{ab^2} \tag{1}$$

Where: F – Destructive load, N;

a, b, l – width and height of sample prism, and distance between supports, respectively, mm;

δ – scaling factor for converting the strength of concrete to the strength of concrete in samples of basic size and shape.

The strength in a series of samples was determined as the arithmetic mean value of the strength of the tested samples in the series for the three samples with the highest strength.

3. Results and Discussion

After conducting the experiment and analyzing the obtained data, a comparative analysis of the influence of the technological parameters of the method of joint mixing of steel fiber-reinforced concrete mixture under volumetric-arbitrary fiber orientation was carried out. The experiments revealed that the nature of the samples' failure with 3 and 9 seconds of vibration during the strength test in bending was predominantly plastic, as opposed to the brittle failure exhibited by samples without fibers. A graph depicting the comparison of the impact of the technological parameters of the joint mixing method of steel fiber-reinforced concrete mixture under volumetric-arbitrary fiber orientation on the flexural strength of the samples is presented in Figure 4.
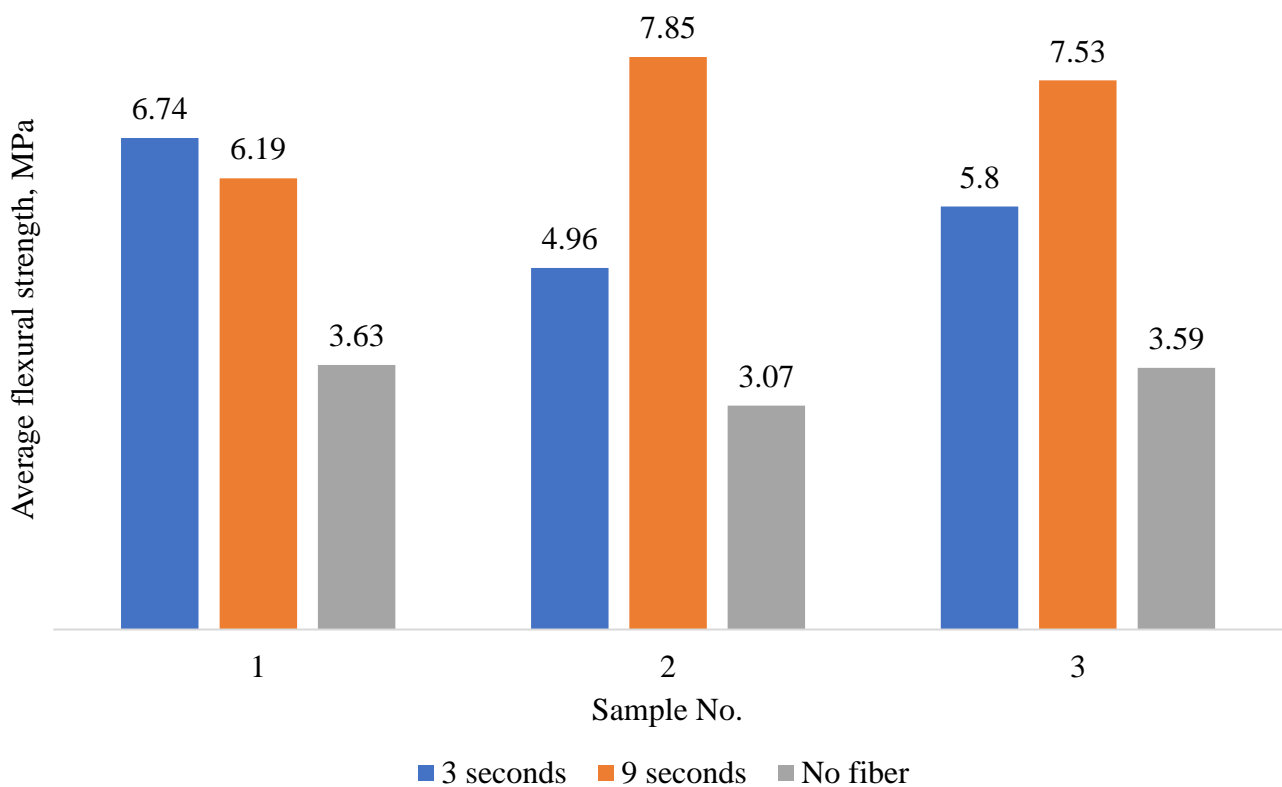

Figure 4 – Effect of the manufacturing technology of steel fiber concrete on its flexural strength

The graph indicates that the flexural strength of samples subjected to 3 seconds of vibration increased on average by 1.7 times (i.e., 70%), while those subjected to 9 seconds of vibration increased by 2.1 times (i.e., 210%). Analyzing the obtained results, it can be concluded that the bending strength of the samples is comparable to that obtained in similar studies [7].

4. Conclusions

The results of the study indicate that the incorporation of steel fibers into the concrete mixture can enhance the material's ductility, leading to a plastic failure mode instead of brittle failure. This observation underscores the potential of steel fiber reinforcement to improve the mechanical properties of concrete, particularly in applications where flexural strength is critical, such as in structural elements subjected to bending loads.

The analysis of the test results confirmed that the method of joint mixing of steel fiber-reinforced concrete with randomly oriented fibers made from used cables increases its mean value of flexural strength. At the same time, the highest flexural strength is exhibited by the concrete mixtures with a vibration time of 9 seconds. The strength of samples made from this type of mixture was found to be 2.1 times higher than that of plain concrete samples based on the test results.

References
1. SP 52-104-2006* Steel fibre reineorced concrete structures. — 2010. — 63 p.
2. Effect of Change in Micro Steel Fiber Content on Properties of High Strength Steel Fiber Reinforced Lightweight Self-Compacting Concrete (HSLSCC) / S. Iqbal, A. Ali, K. Holschemacher, T.A. Bier // Procedia Engineering. — 2015. — Vol. 122. — P. 88–94. https://doi.org/10.1016/j.proeng.2015.10.011
3. Mechanical Properties of Steel-Fiber-Reinforced Concrete / I.U. Khan, A. Gul, K. Khan, S. Akbar, Irfanullah // ICEC 2022MDPI, 2022. — P. 6. https://doi.org/10.3390/engproc2022022006
4. TU 1211-205-46854090-2005 Steel wire fiber for concrete reinforcement. — 2005. — 9 p.
5. GOST 10180-2012 Concretes. Methods for strength determination using reference specimens. — 2013. — 36 p.
6. GOST 29167-91 Concretes. Methods for determination of fracture toughness characteristics. — 2021. — 15 p.
7. Effect of Matrix Composition on Steel Fiber Reinforced Concrete Properties / D.O. Al-Ghamdy, E. Tons, J.K. Wight // Journal of King Saud University - Engineering Sciences. — 1993. — Vol. 5, No. 1. — P. 55–75. https://doi.org/10.1016/S1018-3639(18)30571-3

Information about authors:

Dias Kazhimkanuly – MSc, PhD Student, Department of Civil Engineering, L.N. Gumilyov Eurasian National University, Astana, Kazakhstan, dias27049795@gmail.com

Valeriy Chernavin – Candidate of Technical Sciences, Associate Professor, School of Architecture and Construction, D. Serikbayev East Kazakhstan Technical University, Ust-Kamenogorsk, Kazakhstan, vchernavin58@mail.ru

Author Contributions:

Dias Kazhimkanuly – concept, methodology, resources, data collection, drafting, funding acquisition.
Valeriy Chernavin – testing, modeling, analysis, visualization, interpretation, editing.